Korean J. Chem. Eng., 38(4), 674-691 (2021)
DOI: 10.1007/s11814-021-0755-y
pISSN: 0256-1115
eISSN: 1975-7220

REVIEW PAPER

Hydrogen sulfide removal technology: A focused review on adsorption and catalytic oxidation

Jae Hwan Yang[*,**,†]

*Department of Environmental Engineering, Chungnam National University,
99 Daehak-ro, Yuseong-gu, Daejeon 34134, Korea
**Department of Environmental & IT Engineering, Chungnam National University,
99 Daehak-ro, Yuseong-gu, Daejeon 34134, Korea
(*Received 21 December 2020 • Revised 15 January 2021 • Accepted 26 January 2021*)

Abstract−The principal technologies for H_2S removal are reviewed herein. Two technologies in particular, adsorption and catalytic oxidation, are considered as promising for desulfurization in terms of process simplicity, H_2S removal performance, and operational cost. Nanoporous materials such as activated carbons, zeolites, mesoporous silicas, and metal organic frameworks are extensively used as sorbents because their porous characteristics are suitable for efficient diffusion and capture of H_2S. To improve the H_2S adsorption performance, these materials are frequently modified with functional groups or doped with various metal oxides. For example, representative metal oxide-based catalysts (e.g., vanadium, magnesium, and iron oxides) have been investigated for the selective oxidation of H_2S to elemental sulfur. In this context, the dispersion of active metals onto supports, or the addition of modifying metals, are reasonable strategies for inhibiting catalyst deactivation and enhancing catalytic activity. Emerging studies based on the combination of adsorption and catalytic oxidation have introduced the syntheses of dual-function materials,, such as metal nanoparticle-dispersed or metal-free porous carbons. In conclusion, comprehensive research into catalyst synthesis and performance evaluation must continue in order to develop the most promising technology for H_2S removal.

Keywords: Desulfurization, Nanoporous Sorbent, Metal Oxide-based Catalyst, Dual-function Material

INTRODUCTION

Hydrogen sulfide (H_2S) is found in biogas generated from various landfilled organic waste (e.g., sewage sludge, livestock excretions, food and agricultural waste). Due to its severely corrosive nature, H_2S must be effectively removed from biogas before the latter can be used as an energy source [1]. Chemical industries, such as crude oil or coal processing, also produce H_2S during the hydrodesulfurizing process [2], where uncontrolled emission could cause serious danger to human beings and animals.

The unpleasant odor of H_2S gas can be detected even at a concentration of 0.5 ppb [3], its low odor threshold leading to many complaints from residents close to landfills. In addition, the inhalation of H_2S triggers respiratory health problems [2], with a comprehensive study on human health indicating rapid fatality after exposure to air contaminated with 700 ppm H_2S [4]. The perils of H_2S are also related to attack of the neural system and internal organs such as the liver and kidneys [5]. Moreover, the high corrosiveness of H_2S can damage concrete surfaces, sewer pipes, and production facilities [6,7].

The adverse effects of H_2S exposure are summarized in Table 1. Due to this high risk, exposure is strictly limited by regulatory agencies. For example, the US Environmental Protection Agency (EPA) has recommended an oral reference dose (RFD) of 0.003 mg/kg/day and an inhalation reference concentration (RFC) of 0.001 mg/m^3 [2]. To protect employees, the Occupational Safety and Health Administration (OSHA) asserted that industrial workplaces should maintain H_2S levels below 20 ppm during the working day [2]. For drinking water, the H_2S concentration is restricted to the level of 0.05 mg/l by the US National Interim Secondary Drinking Water Regulations (NISDWR) [8].

Considering the negative effects of H_2S inhalation and the strict regulations on emissions, it is necessary to develop efficient control technologies for environmental protection. To date, various desulfurization technologies have been studied, including stripping [9], absorption [10], microbiological treatment [11], adsorption [12], and catalytic oxidation [13]. Among these, adsorption is generally regarded as promising due to its superior performance, economy, operational simplicity, and low toxicity [2,14-16]. In addition, many researchers have focused on the catalytic removal of H_2S since it can be selectively oxidized to elemental sulfur, which is reusable in a wide range of industries [17].

Many research efforts have been devoted to enhancing the current H_2S removal technologies [2,14,15,17-21]. Nevertheless, although adsorption and catalytic oxidation have been separately reviewed, a comprehensive article that covers the characteristics, advantages, and drawbacks of these two prominent technologies is still needed. With this in mind, the present review focuses on the recent progress in adsorption and catalytic oxidation for H_2S removal, along with the introduction of novel materials at the cutting edge of nano-

†To whom correspondence should be addressed.
E-mail: yjh98@cnu.ac.kr

Table 1. Hazards according to the level of H_2S exposure [4]

Exposure (mg/m^3)	Health effects
0.011	Odor threshold
2.8	Bronchial constriction in asthmatic individuals
5.0	Increased eye complaints
7 or 14	Increased blood lactate concentration, decreased skeletal muscle citrate synthase activity, decreased oxygen uptake
5-29	Eye irritation
28	Fatigue, loss of appetite, headache, irritability, poor memory, dizziness
>140	Olfactory paralysis
>560	Respiratory distress
≥700	Death

technology and material science. Other H_2S removal techniques, such as absorption, cryogenic distillation, and membrane separation, are beyond the scope of the present article. In addition, the present article addresses the perspectives of future research and provides guidance for the development of desirable materials for H_2S removal.

ADSORPTION

An adsorption process is used to remove contaminants from gases using solid sorbents. This well-proven gas purification technology has been successfully adopted in various areas for environmental protection such as biogas separation, CO_2 capture, purification of H_2 and CH_4, and H_2S removal [22]. Because the adsorbates are adsorbed onto the sorbent surfaces during this process, the adsorption capability is significantly affected by the surface area of the sorbent. Adsorption is classified as physical adsorption (physisorption) or chemical adsorption (chemisorption) according to the nature of the bonding between the gaseous molecules and the sorbents. Physisorption takes place when the gas molecules are attracted to the sorbent surface by van der Waals forces without sharing electrons between the adsorbates and the surface of the sorbent [16]. Low temperature is favorable for avoiding desorption of the adsorbed molecules, and the activation energy is small in physisorption [15]. In contrast, chemisorption requires a relatively high activation energy to induce chemical reactions involving the formation of covalent bonds between the adsorbed molecules and the adsorbent surface.

Activated carbons [23-28], zeolites [29,30], mesoporous silicas [31], and metal organic frameworks (MOFs) [32-35] have been extensively studied for H_2S adsorption. These materials generally have substantial adsorption capacity due to their porous structure, high surface area, and large pore volume.

Another approach is the use of metal oxides to adsorb H_2S via chemical reactions which lead to the formation of metal sulfides via the following reaction [36]:

$$MO_x + xH_2S \rightarrow MS_x + xH_2O \quad (1)$$

where M is the metal. This reaction mostly takes place at low or moderate temperatures (25-300 °C). Representative metal oxides for H_2S adsorption include iron oxide [31,36-38], copper oxide [39], and zinc oxide [40]. Although these materials are thermodynamically feasible for desulfurization, their relatively low surface area compared with that of nanoporous materials is a major drawback of the metal oxide-based sorbents [41]. Hence, it is a reasonable strategy to disperse metal oxides on high-porosity support materials [42-46]. In the present section, the discussion will focus on representative nanoporous materials used for desulfurization, while the metal oxide-based sorbents will be discussed later.

1. Activated Carbon

Activated carbons (AC) have been widely used for desulfurization due to their excellent surface area (>1,000 m^2/g) and high degree of microporosity [16,24]. For the preparation of AC, carbon is usually activated by pyrolyzing carbonaceous precursors such as coal, wood, coconut shell, or peat [20]. This step forms charcoal with pores that are too small for practical use, so further activation is performed by steam or CO_2 to generate accessible pore structure [16]. The high surface area of AC generally favors its adsorption capacity by providing sufficient adsorption sites [47]. However, the adsorption properties are not solely determined by the surface area; rather, the physical and chemical properties of the AC significantly affect the adsorbate-adsorbent interaction [27]. With this in mind, ACs impregnated with various chemical agents have been synthesized to improve the adsorption performance in H_2S removal [47-51].

Surface acidity is one of the factors affecting the adsorption behavior of ACs [47,48,51]. For example, Turk et al. prepared granular activated carbon (GAC) impregnated with KOH or NaOH to obtain caustic carbon with an enhanced H_2S adsorption capacity that was 1.3-2.7 times higher than that of the pristine AC [48]. Interestingly, the injection of ammonia gas into the gas stream was also found to be advantageous for H_2S adsorption, with an enhancement in the adsorption capacity by a factor of 3 or more compared to that of the caustic carbon. It was suggested that ammonia acts as a catalyst to facilitate the oxidation of H_2S via the following reactions:

$$3NH_3 + 3H_2S \leftrightarrow 3NH_4HS \quad (2)$$

$$NH_4HS + 1.5O_2 \rightarrow NH_4HSO_3 \quad (3)$$

$$NH_4HSO_3 \leftrightarrow NH_3 + SO_2 + H_2O \quad (4)$$

$$2NH_4HS + SO_2 \rightarrow 3S + 2NH_3 + 2H_2O \quad (5)$$

where the rate determining step for the catalytic reactions was Eq. (3).

The influence of surface property on the removal of H_2S has been extensively studied by Bandosz et al. [24,27,52-55]. The presence of pores with specific sizes, along with surface acidity provided by alkali metals, was shown to be beneficial for the removal of H_2S by stimulated oxidation [52]. In addition, surface-oxidized ACs prepared with nitric acid or ammonium persulfate revealed a correlation between the heat of H_2S adsorption (Q_{ads}) and the structural parameters of the carbon surface [53]. The values of Q_{ads} for the modified samples ranged between 39 and 47 kJ/mol, which was 1.9-2.3 times higher than that obtained for carbon black [54]. Further, a study on the effect of the presence of surface functional groups revealed that the adsorption of H_2S was improved by carbons with surface functionality [54]. This was attributed to the adsorption of water by the surface groups, which facilitates the oxidation of H_2S to elemental sulfur or water-soluble sulfur species. The effect of surface basicity of AC was also investigated by Adib et al., who demonstrated that wood-based ACs impregnated with urea could oxidize H_2S to water-soluble H_2SO_4 via basic nitrogen groups that were highly dispersed in the micropores of the carbon matrix [55]. Thus, the basic compounds lead to the dissociation of H_2S into the reactive HS^- ion, which is readily oxidized to sulfur oxides and sulfuric acids. However, the adsorption capacity of H_2S was decreased by about 10% compared with that of the unmodified AC, presumably due to the reduction of surface area after urea impregnation. Surface modification of AC using 3-aminopropyltriethoxysilane (APTES) has been performed by [56]. The enhanced basicity due to the -NH_2 groups significantly increased the breakthrough capacity of H_2S removal to 16.84 mg/g with an inlet H_2S concentration of 1,600 ppm, which was 3.55 times higher than that of the unmodified AC (4.74 mg/g). The presence of water in the gas stream and high temperatures were found to decrease the H_2S removal performance, while the presence of oxygen improved H_2S removal.

The feasibility of repetitive AC re-use has been investigated via adsorption/regeneration cyclic tests [57]. After H_2S adsorption on coconut shell-based AC, the used AC was regenerated by washing with cold or hot water. After the first regeneration step, the AC displayed a significant decrease of ~60% in the H_2S adsorption capacity, which then remained at a similar level in subsequent runs. This behavior was explained by the strong adsorption of elemental sulfur and sulfuric acid in the carbon micropores, resulting in irreversible exhaustion of the adsorption capacity. It was also found that hot water was slightly more effective at removing the elemental sulfur that was deposited in the carbon pores. The low regeneration capacity of exhausted AC was also reported by [24], thus indicating a negative prospect for the potential application of AC in H_2S removal.

Various metal oxides have also been used to functionalize AC for enhanced H_2S removal. For example, Fauteux-Lefebvre et al. examined the H_2S adsorption performance of carbon nanofilament (CNF) impregnated with iron (Fe) nanoparticles [58]. In this procedure, wet impregnation with iron was preceded by acid treatment to decrease the hydrophobicity of the CNF and generate metal anchor sites. The adsorbent loaded with 20 wt% Fe exhibited the highest breakthrough capacity of 7.42 g H_2S/100 g CNF at 300 °C. It was revealed that acid treatment was influential for uniform dispersion of the nanosized Fe particles. Similarly, AC loaded with manganese dioxide (MnO_2) has been prepared by wet impregnation for use in desulfurization [59]. Although the surface area of the modified AC was substantially reduced, the H_2S breakthrough capacity was significantly increased to 110.7 mg/g for the adsorbent with 50 wt% MnO_2 at 20 ppm H_2S, compared to 13.8 mg/g for the unmodified AC under the same testing conditions. Meanwhile, Balsamo et al. investigated the effect of combined ZnO and CuO dispersion in AC, with atomic ratio of Cu : Zn ranging from 0 : 1 to 1 : 1 [60]. The highly-dispersed metal particles did not noticeably block the pores in the AC support, and dramatically enhanced the adsorption capacity. Importantly, the H_2S sorption capacity was found to gradually improve with increasing CuO addition. Hence, it was considered that the diffusional limitation commonly encountered in ZnO-based sorbents due to the formation of a dense, thin ZnS overlayer was reduced due to the replacement of Zn by Cu [61]. Moreover, the sorbents with higher Cu fraction displayed higher metal oxide utilization factor and lower metal sulfate decomposition temperature during desulfurization. The latter characteristic is beneficial for the regeneration of spent sorbents. The H_2S removal performance of various ACs under a range of conditions is summarized in Table 2.

2. Zeolites

Zeolites are generally defined as porous aluminosilicate minerals with crystalline structure built up from SiO_4 and AlO_4 tetrahedra which are interlinked via the sharing of oxygen atoms to form ordered pore channels at a molecular level [16,62]. Due to these unique frameworks, zeolites have long been used in various sepa-

Table 2. Comparison of the H_2S removal performance of various carbon-based adsorbents

Adsorbent	Feed gas	Temperature (°C)	Breakthrough capacity (g-H_2S/g-sorbent)	Reference
Wood-based commercial AC	H_2S: 3,000 ppm (Air base), RH: 80%	25	0.295	[52]
Wood-based, H_3PO_4-activated AC	H_2S: 10,000 ppm, (Air base), RH: 80%	20	0.047	[54]
Urea-impregnated AC	H_2S: 3,000 ppm (Air base), RH: 80%	25	0.298	[55]
Coconut shell-based AC	H_2S: 3,000 ppm (Air base), RH: 80%	25	0.125	[57]
Fe nanoparticle-impregnated CNF	H_2S: 500 ppm (He base)	300	0.074	[58]
MnO_2-loaded AC	H_2S: 20 ppm (N_2 base)	40	0.111	[59]
ZnO-CuO dispersed AC	H_2S: 3,000 ppm (N_2 base)	30	0.050	[60]

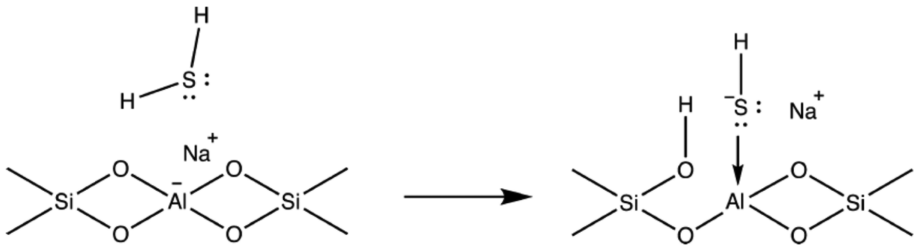

Fig. 1. Schematic of dissociative H_2S adsorption on an aluminosilicate zeolite [16].

ration and gas purification processes [62-66]. The adsorption property of zeolites is affected by the size, shape, and arrangement of the pores, the Si/Al ratio of the framework, and the nature of the cations that reside within the pore structure [67,68]. The polarizable nature of aluminosilicate zeolites allows dissociative adsorption of H_2S (Fig. 1), thus leading to the application of various zeolites in desulfurization processes.

Faujasite (FAU)-type zeolites have been applied for H_2S adsorption to reveal the adsorption mechanism and the influence of the Si/Al ratio [30]. Characterization by infrared spectroscopy suggested that the dissociative adsorption of H_2S to form -OH and -SH groups is favored when Al-rich NaX-type zeolites (Si/Al<2.5) are used. By contrast, physical adsorption was found to be the primary mechanism of H_2S removal in the case of NaY-type zeolites with Si/Al>2.5, which have fewer Na^+ cations on the walls of the α-cages. Hence, it was considered that the abundance of Na^+ cations in the NaX zeolites plays an important role in the dissociation of H_2S into HS^- and H^+. The molecular adsorption of H_2S on the surfaces of zeolites with high Si/Al ratios has been confirmed by Garcia and Lercher, who examined ZSM-5 zeolites with an Si/Al ratio of 35.5 and proposed models for the adsorption of H_2S [69]. They observed that H_2S molecules were adsorbed onto the zeolite surface without any dissociation, such that hydrogen bonds were formed between S and H, while coordinative bonds were formed between S and Na.

Theoretical calculations and molecular simulations using Grand Canonical Monte Carlo and molecular dynamics were performed by Cosoli et al. to study H_2S removal by FAU (NaX, NaY)-, LTA-, and MFI-type zeolites [70,71]. The results indicated that the hydrophilic zeolites favored H_2S adsorption due to their high isosteric heat of adsorption. It was also suggested that the NaY framework would be the best candidate for H_2S removal. When a simulated biogas mixture was considered, a significant decrease in the adsorption capacity of H_2S was indicated for the LTA- and MFI-type zeolites due to competitive adsorption of CO_2, CH_4 and H_2S. Quantum mechanical calculations based on density functional theory (DFT) were also applied to evaluate the feasibility of multivalent cation-exchanged FAU zeolites as selective adsorbents for H_2S [72]. Computations on the adsorption energy of H_2S and other gas components (N_2, CO, H_2O, and CO_2) showed that water tends to be strongly adsorbed on these zeolite surfaces. In addition, the gadolinium-exchanged Y zeolite (Ga-Y) showed the largest difference between the adsorption energy of H_2S and CO. Based on these modeling results, a two-step process was suggested as a reasonable strategy in which the moisture contained in the tail gas was first removed by the most hydrophilic zeolite (Cu-Y), followed by desulfurization using Ga-Y.

In other studies, zeolites modified with various metal cations have been prepared by ion exchange or wet impregnation for use in desulfurization [73-75]. For example, Pavlova et al. synthesized granule-type zeolite A and X in which Na^+ cations were exchanged with various cations such as K^+, H^+, Li^+, Mg^{2+}, Ca^{2+}, and La^{3+} [74]. Dynamic tests indicated dramatically enhanced H_2S absorption capacity for the zeolites A exchanged with Li^+, Mg^{2+}, and Ca^{2+} to about four or five times compared to that of the unmodified zeolite A. By contrast, an improvement in H_2S adsorption due to cation exchange was not observed in the case of zeolite X. Rather, the zeolites X modified with H^+, Mg^{2+}, Ca^{2+}, and La^{3+} showed significantly lower capacity than that of the pristine zeolite X. These results were attributed to the higher accessibility of the zeolite A cavity towards the exchange of Na^+ with Li^+, Mg^{2+}, and Ca^{2+} cations [76]: it was considered that the effective size of the entrance windows, as well as the cation positions within the zeolite cavities, were modified by cation exchange, thus improving the accessibility of the zeolite cavities and leading to fast diffusion of H_2S molecules. Micoli et al. investigated the adsorption property of zeolites 13X modified with Cu^{2+} or Zn^{2+} via ion exchange or the incipient wetness method [73]. The breakthrough test performed at 8 ppm of H_2S revealed that the Cu^{2+}-exchanged zeolite exhibited the highest adsorption performance with the 39.9 mg-H_2S/g-sample, which was 13 times higher than that of the unmodified zeolite 13X. The improved H_2S adsorption capacity was attributed to the strong affinity of Cu^{2+} for S^{2-} ions. Kumar et al. examined the removal of H_2S from gas mixture gases containing He, N_2, CO, CO_2, or H_2O using Ag^+- or Cu^{2+}-exchanged faujasites (X and Y) to indicate a definite increase in the H_2S adsorption capacity in the presence of all other species when each of the Ag^+-exchanged zeolites were used [75]. In the case of the Cu^{2+} exchanged zeolites, however, H_2S could not be removed in the presence of 2% CO, although efficient H_2S removal was achieved in the presence of N_2, CO_2, and H_2O. DFT calculations indicated that the adsorption energy of CO on CuY was higher than that of H_2S, which explained the poor adsorption of H_2S in the presence of this gas. The H_2S breakthrough capacity of the various zeolite-based sorbents that have been studied for use in desulfurization are presented in Table 3.

3. Mesoporous Silica

A series of mesoporous silica materials designated MCM was first synthesized at the Mobil Corporation Laboratories in the early 1990s [77]. Since then, other types of mesoporous silica, such as the FSM, SBA, KIT, AMS, and MSU series, have been reported

Table 3. Comparison of the H_2S removal performance of various zeolite-based adsorbents

Adsorbent	Feed gas	Temperature (°C)	Breakthrough capacity (g-H_2S/g-sorbent)	Reference
13X	H_2S: 80 ppm (N_2 base)	25	0.075	[20]
Ag-exchanged 13X	H_2S: 100 ppm (N_2 base)	25	0.064	[75]
Cu-exchanged 13X	H_2S: 8 ppm (He base)	40	0.040	[73]
Ag-exchanged NaY	H_2S: 100 ppm (N_2 base)	25	0.058	[75]
Cu-exchanged NaY	H_2S: 100 ppm (N_2 base)	150	0.038	[75]
Ca-exchanged NaA	H_2S: 1 ppm (CH_4 base)	25	0.005	[70]

[78-82]. Mesoporous silicas exhibit distinctive characteristics of high surface area, uniform pore size, and surface chemistry that can be tailored via controlled reaction conditions, structure-directing agents, or surface-modifying chemicals [20]. These features enable the application of mesoporous silicas to various adsorption processes [83-85]. However, mesoporous silica itself is not appropriate for H_2S adsorption due to the low affinity of the silica surface toward H_2S; hence, surface-modification with appropriate functional groups is required [20].

Amines are among the most studied materials for the functionalization of mesoporous silicas [20]. For example, Huang et al. synthesized MCM-48 grafted with (3-aminopropyl) triethoxysilane for H_2S adsorption [86]. Weak chemical interaction between the basic amine groups and the acidic H_2S gas enabled the formation of NH_3^+-HS^- groups, thus resulting in a high adsorption capacity of 21 mg/g at 25 °C. Moreover, the sorbent could be completely regenerated by pressure- or temperature-swing methods. Also found was that the H_2S adsorption performance was barely affected by the presence of H_2O and CH_4. Meanwhile, Xu et al. investigated the low-temperature removal of H_2S by polyethylenimine (PEI)-modified MCM-41 [87]. The 3-nm pore size of mesoporous MCM-41 was advantageous for loading the PEI as nanoparticles, which was expected to result in enhanced H_2S adsorption performance compared with that of the bulk PEI particles. The high dispersion of PEI in the mesopores allowed the H_2S effective access to the numerous amine groups of PEI [88] and provided an improved adsorption capacity of ~0.234 mg/g-sorbent compared to that of a commercial ZnO (0.148 mg/g-ZnO). This was attributed to the moisture resistance of the sorbent and the finely distributed functional groups. Moreover, the adsorption performance of the PEI-loaded MCM-41 was found to remain stable even under repetitive cyclic adsorption/desorption tests. Nevertheless, the adsorption capacity should be further enhanced for practical application of the sorbent. Wang et al. also used PEI to prepare functionalized mesoporous silicas including MCM-41, MCM-48, and SBA-15 molecular sieves for use in desulfurization [89]. It was found that the H_2S breakthrough and saturation capacity were dramatically increased as the process temperature was decreased from 75 to 22 °C. The type of molecular sieve and the amount of PEI loading significantly affected the adsorption performance, with the best breakthrough and saturation capacity being obtained for SBA-15 loaded with 50 and 65 wt% PEI, respectively. The regeneration and stability tests revealed that the SBA-15 with 50% PEI could be effectively regenerated with desorption rate of >83% at mild temperatures and retained a stable saturation capacity of 62.1 mg-H_2S/g-sorb. after 8 cycles, which corresponds to 92% of the fresh sorbent.

One of the influential factors affecting H_2S adsorption performance is the degree of loading of active metal species on the mesoporous silica support. With this in mind, Wang et al. first synthesized mesoporous silica SBA-15 grafted with ZnO nanoparticles using incipient wetness impregnation and ultrasonic treatment [90], followed by loading with 3.04 wt% zinc to provide an excellent H_2S removal ability down to the ppb level, with a maximum H_2S breakthrough capacity of 463 mg-H_2S/g-sorbent at 25 °C. The enhanced capacity, which was ~12 times higher than that of SBA-15 with 0.5 wt% Zn, originated from the efficient utilization of ZnO enabled by the homogeneous dispersion of the metal nanoparticles into both the mesopores and micropores of the SBA-15. However, excessive addition of ZnO was found to be rather detrimental to H_2S removal. This was attributed to physical blockage of the SBA-15 pores by the excess ZnO which led, in turn, to an increase in pH that facilitated further pore plugging by reaction products, thus resulting in limited gas diffusion. A similar post-synthesis grafting method has been used to prepare iron-oxide-modified SBA-15 in which nanosized Fe_2O_3 particles were highly dispersed on the outside surface and inside the pore channels due to ultrasonic-assisted treatment [90]. The maximum H_2S uptake capacity of 745 mg-H_2S/g-sorbent at 25 °C was obtained with 31.3 wt% Fe. The enhanced performance was attributed to the smooth mass transfer of H_2S molecules through the pore channels followed by efficient gas-solid reactions between the H_2S and hydrated Fe_2O_3 nanoparticles. However, this was further enhanced by a catalytic effect in which the iron sulfides formed by the reaction between Fe_2O_3 and H_2S were further reacted to sulfur in the presence of sufficient oxygen, thus recovering the Fe_2O_3 active sites.

Copper-oxide incorporated mesoporous silicas have also been studied for H_2S removal. Ozaydin et al. synthesized copper-modified MCM-41 via one-pot hydrothermal and post-impregnation route [91]. These materials showed higher H_2S adsorption capacity than that of the pure CuO primarily due to the uniform dispersion of copper species over the high surface area of the MCM-41. The sulfur retention capacity of the sorbent prepared by the impregnation method was higher than that of the directly-synthesized material, probably due to the non-utilization of copper atoms inside the MCM-41 lattice of the sorbents synthesized by the one-pot method. However, the practical application of these sorbents in a desulfurizer is doubtful because the experiments were performed at a high temperature of 500 °C, which would increase the opera-

Table 4. Comparison of the H_2S removal performance of various types of mesoporous silicas

Adsorbent	Feed gas	Temperature (°C)	Breakthrough capacity (g-H_2S/g-sorbent)	Reference
PEI-impregnated MCM-48	H_2S: 4,000 ppm, H_2: 20% (N_2 base)	22	0.063	[89]
PEI-impregnated SBA-15	H_2S: 4,000 ppm, H_2: 20% (N_2 base)	22	0.103	[89]
ZnO-supported SBA-15	H_2S: 1,000 ppm (Air base)	25	0.436	[90]
Fe_2O_3-supported SBA-15	H_2S: 1,000 ppm (Air base), RH: 55%	25	0.701	[90]
Copper-incorporated MCM-41	H_2S: 10,000 ppm, H_2: 10% (He base)	500	0.079	[91]
ZnO-supported MSU-1	H_2S: 5% (CH_4 base)	25	0.042	[81]

tion costs. Moreover, the experiments were performed in an infeasible atmosphere of 10% H_2, which benefits the chemisorption of H_2S by converting copper oxide into metallic copper. The H_2S breakthrough capacity of the various types of mesoporous silica is summarized in Table 4.

4. Metal Organic Frameworks (MOFs)

MOFs are porous materials which consist of organic linkers coordinated by metal ions or nano-metallic clusters [92]. Their distinctive porous frameworks enable MOFs to encage metal atoms or the metal oxide clusters by forming coordinative bonds [16]. Typically, MOF pore sizes are distributed within the range of 3-20 Å, which belongs to the micropore regime [93]. However, the tailored design of MOFs to modify the size and shape of the pores and to provide proper functionality is also possible. These characteristics allow MOFs to be used as adsorbents for various gas molecules (H_2, CH_4, CO_2, etc.) [94-98]. The application of MOFs for desulfurization has also been actively studied [99-102], and important results of these studies are summarized below along with the present author's interpretations.

Hamon et al. first investigated the H_2S adsorption capacity of six different MOFs [103]. They synthesized MIL-series MOFs with small pores (e.g., MIL-47(V^{IV}), MIL-53(Al^{III}, Cr^{III}, Fe^{III})) and large pores (e.g., MIL-100(Cr) and MIL-101(Cr)). The first class of MOFs have BET surface areas of ~1,000 m^2/g and consist of corner-sharing chains of $M^{IV}O_6$ or $M^{III}O_4(OH)_2$ octahedra connected through terephthalate moiety. The large-pore MOFs are built up from trimers of chromium octahedra with trimesate or terephthalate moiety that produce ordered mesoporous structures with surface areas of greater than 2,000 m^2/g. Adsorption isotherm measurements at room temperature showed that these materials could take up very high amount of H_2S, with a maximum quantity of 1,309 mg/g for the large-pore MIL-101. The regeneration study revealed that the H_2S adsorption capacity of the small-pore MOFs was fully recoverable by desorption, whereas that of the large-pore MOFs was not fully reversible. The irreversibility of adsorption by MIL-100 and MIL-101 appears to be related to strongly adsorbed H_2S molecules or to a partial destruction of the framework. However, the application of MIL-101 for H_2S removal need not be limited by this result since modeling work has suggested that full regeneration of MIL-101 is possible under very low H_2S partial pressure of ~0.1 kPa, which is much closer to those of actual hydrogen sulfide emission streams [104].

Functionalization is also a common strategy for modifying MOFs by grafting functional moieties within the porous channels. As with the cases of AC and mesoporous silica, amine is a preferred functional group for MOF modification. For example, Wang *et al.* prepared Zn-based IRMOF-3 for the adsorptive removal of various sulfur compounds at ambient temperature [105]. Characterization revealed that the H_2S adsorption was related to the following two mechanisms: (i) an acid-base interaction between the amino group and H_2S molecules, and (ii) a chemical reaction between zinc in the MOF and sulfur in H_2S to form ZnS. Nevertheless, the H_2S breakthrough capacity was very limited, with a maximum of 15.7 mg/g, which is much lower than that of other MOFs [103]. Additionally, the regenerability of IRMOF-3 is doubtful because the chemical adsorption of H_2S would seriously damage the MOF framework due to the substitution of the Zn-bonded structural oxygen by the sulfur of H_2S. Meanwhile, Vaesen et al. investigated amino-functionalized titanium MIL-125 for the elimination of CO_2 and H_2S from a simulated biogas mixture containing these gases along with CH_4 [106]. The modified sorbent exhibited an enhanced H_2S adsorption at low pressure ranges compared to that of the parent MIL-125(Ti). Characterization by in-situ infrared spectroscopy revealed that hydrogen bonds were formed between the H_2S as a proton donor and the amino group of MIL-125(Ti)-NH_2 as a proton acceptor. Additionally, molecular dynamics simulations using the Grand Canonical Monte Carlo method predicted that the selectivity of both H_2S and CO_2 over CH_4 would be significantly improved by the amine functionalization. Given the thermal stability up to 100 °C in the presence of moisture and the excellent reversibility upon repeated use, MIL-125(Ti)-NH_2 is regarded as a potential adsorbent for the concomitant removal of CO_2 and H_2S from biogas streams.

The influence of activation and adsorption temperature on H_2S removal has been investigated using Cu-based MOF-199 [107]. The breakthrough H_2S uptake reached a maximum at an activation temperature of 180 °C with complete removal of the residual solvents used for the synthesis of MOF-199. The positive effect of activation upon the adsorption performance of H_2S has also been examined by [108]. The H_2S adsorption performance was also found to increase as the adsorption temperature was increased from 30 to 80 °C, thus suggesting that a chemical reaction occurred between the H_2S and copper sites on the surface of the MOF-199 to form CuS [107]. However, the disappearance of characteristic peaks in the XRD spectrum after H_2S adsorption indicated that the strong chemical interaction seriously deformed the MOF framework. Therefore, MOF-199 is unlikely to be a promising adsorbent for H_2S removal due to its poor regenerability.

Table 5. Comparison of the H_2S removal performance of various types of MOFs-based sorbents

Adsorbent	Feed gas	Temperature (°C)	Saturation capacity (g-H_2S/g-sorbent)	Reference
MIL-101(Cr)	Pure H_2S, p=2.0 MPa	30	1.31	[103]
MIL-53(Fe)	Pure H_2S, p=1.6 MPa	30	0.291	[103]
MIL-47(V)	Pure H_2S, p=1.6 MPa	30	0.498	[103]
Amino-functionalized IRMOF-3(Zn)	H_2S: 0.1 ppm (N_2 base)	30	0.016	[105]
Amino-functionalized MIL-125(Ti)	Pure H_2S, p=1.0 MPa	30	0.426	[106]
Ni-CPO-27	Pure H_2S, p=0.1 MPa	30	0.409	[108]

However, when Belmabkhout et al. studied a series of isostructural MOFs with soc-topology for use in the separation of H_2S from refinery off-gases (ROG) or natural gas (NG), the Ga- and Al-containing MOFs were found to be suitable for H_2S removal due to their structural integrity and adsorption performance [109]. Additionally, GCMC simulations showed that the Ga-soc-MOF was highly selective toward olefins and paraffins over CH_4, which is desirable for the production of polymers from ROG or NG [110].

More recently, new classes of MOFs have been synthesized and employed as next-generation adsorbents for H_2S removal. In particular, sub-classes of MOFs such as zeolitic imidazolate frameworks (ZIFs) [111], covalent-organic frameworks (COFs) [112], and porous aromatic frameworks (PAF) [113] have recently been synthesized and could also be explored for H_2S adsorption. However, although many studies have reported the use of MOFs for desulfurization, it is difficult to compare the capacity of various MOFs directly because the reported performance data have been obtained under various constrained experimental conditions of H_2S partial pressure, relative humidity, and outlet breakthrough concentration. To overcome this limitation, there is a need for a comprehensive study ranging over the various factors and including reusability. The H_2S saturation capacity of the various MOF-based sorbents is summarized in Table 5.

CATALYTIC OXIDATION

In contrast to adsorption, catalytic oxidation is used to remove H_2S via selective oxidation to elemental sulfur by catalysts in the oxygen-containing atmospheres. This method is employed in the Claus process, first patented in 1883 [114]. In this process the feed gases are usually composed of H_2S, CO_2 and H_2O along with minor fractions of N_2, HNH_3, and hydrocarbons [115]. The conversion of H_2S to sulfur occurs in two reaction stages, as shown in Fig. 2.

In the first stage, one-third of the H_2S is converted to SO_2 in a combustion chamber operating at high temperatures, according to the following equation:

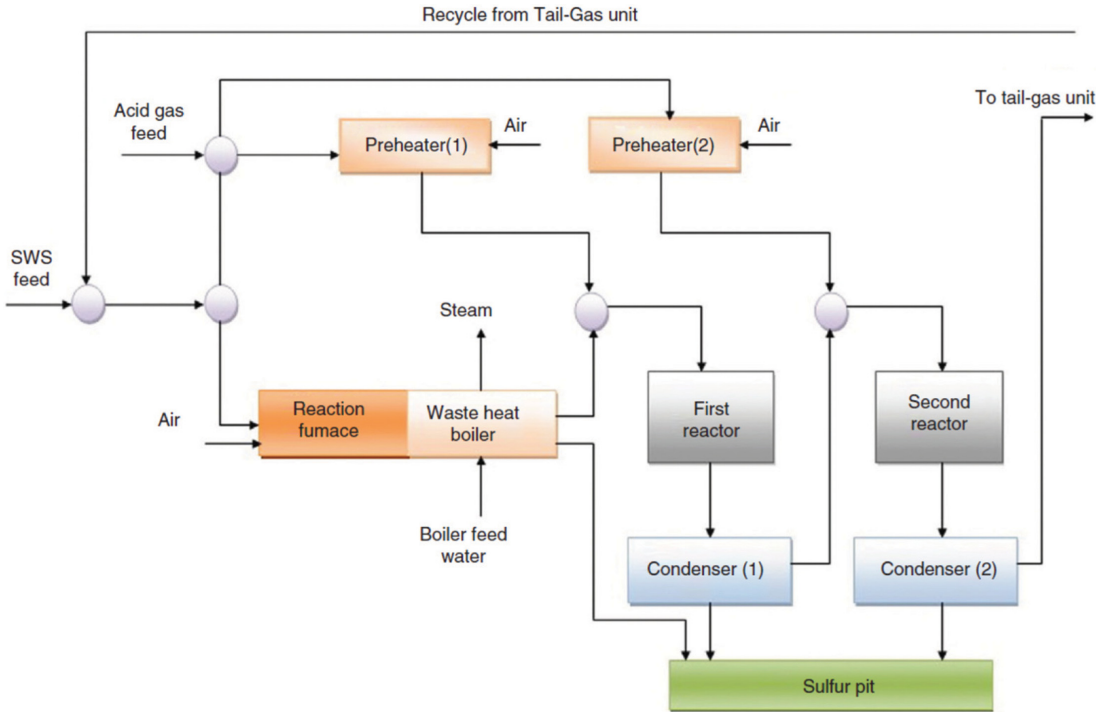

Fig. 2. Flow diagram of two-stage Claus process [119].

$$H_2S+3/2O_2 \rightarrow SO_2+H_2O \quad (6)$$

Although this reaction is thermodynamically favorable (ΔG_o^r=−518 kJ/mol), the conversion efficiency is poor below 1,000 °C [116]. Therefore, it is required to maintain process temperature in the range of 1,000-1,200 °C to obtain the highest yield [117]. The products and remaining H_2S then enter the second reactor, where elemental sulfur is produced by the following reaction [118]:

$$SO_2+2H_2S \rightarrow 2H_2O+3/2S_2 \quad (7)$$

Because this reaction is thermodynamically non-spontaneous (ΔG_o^r= +47 kJ/mol), the tail gas (the off-gas from the Claus process) contains 3-5% of the initial H_2S [17]. Owing to the recently strengthened regulations, this must be treated further to remove the unreacted H_2S. Numerous cleaning technologies have been studied and applied for the tail gas treatment, including absorption, adsorption, wet oxidation, and selective catalytic oxidation [119]. Among these, selective catalytic oxidation has received recent research attention due to the excellent sulfur yield and low cost [17]. In this technique, H_2S is directly converted to elemental sulfur via selective catalytic oxidation by the following irreversible reaction:

$$H_2S+1/2O_2 \rightarrow S+H_2O \quad (8)$$

The key challenge in selective catalytic oxidation is to avoid the reverse Claus reaction and deep oxidation of H_2S by which undesirable sulfur dioxide is produced according to the following reactions [120]:

$$3S+2H_2O \rightarrow 2H_2S+SO_2 \quad (9)$$

$$H_2S+3/2O_2 \rightarrow SO_2+H_2O \quad (10)$$

Therefore, water vapor and the ratio of H_2S/O_2 play an important role in the H_2S conversion and sulfur selectivity.

Various metal oxides have been studied as active substances of catalysts for the selective catalytic oxidation of H_2S [121-127]. Among these, V_2O_5, MgO, and Fe_2O_3 can be considered as promising due to their catalytic activity and selectivity [17,128-130]. The following sections summarize the key results of studies dealing with the catalytic removal of H_2S using metal oxide-based catalysts.

1. Vanadium Oxide-based Catalysts

In the last decades, many researchers have studied vanadium oxide-based materials and suggested V-containing oxides as candidate catalysts for the selective oxidation of H_2S to S [122,131-138]. In particular, Davydov et al. have extensively investigated the catalytic activity and selectivity of various metal oxides to indicate that V_2O_5 displays the best performance in terms of H_2S conversion and S selectivity [139]. A study by Machej et al. [140] revealed that vanadium species are present as a mixture of a two-dimensionally dispersed amorphous phase and V_2O_5 crystallites in supported catalysts. In addition, characterization by in-situ Raman and XAS spectroscopies suggested that the formation of V^{5+}-O-V^{4+} pairs due to the presence of V_4O_9 was beneficial for higher S selectivity [134, 135]. These pairs play an important role in enhancing the redox property of the catalytic reactions because the coexistence of V^{4+} and V^{5+} species leads to a higher concentration of oxygen vacancies [141].

The activity of the vanadium-based catalysts is significantly improved when bulk V_2O_5 is supported on proper supports (e.g., SiO_2, Al_2O_3, TiO_2, zeolite). For example, Li and Chien [142] investigated the effects of various supports for vanadium-based catalysts to indicate that TiO_2-supported V_2O_5 displays the highest H_2S conversion capability and S selectivity. The positive effect of the TiO_2 support is attributed to its strong interaction with vanadium, which accelerates the formation of oxygen vacancies and rapid catalyst regeneration from V^{4+} to V^{5+} [141]. Oxygen vacancies facilitate the dissociative adsorption of O_2, by which active oxygen species (e.g., O_2^-, O_2^{2-}, O^-) for catalytic reactions are generated [143].

The promotional effects of metal oxides in V-containing catalysts have been studied by many researchers. Soriano et al. [138] investigated the influence of alkali metal (Cs, Li, K, Na) incorporation in V_2O_5-based catalysts to indicate the highest activity for Na-doped V_2O_5, with an excellent S selectivity of >98% when the process temperature was less than 220 °C. It was also suggested that V_4O_9 and $Na_{0.33}V_2O_5$ were formed as active and selective phases during the catalytic reactions, and these were responsible for the presence of V^{4+}-O-V^{5+} pairs. Meanwhile, Kim et al. [144] studied the effect of molybdenum addition upon V_2O_5-supported TiO_2 to reveal significant improvement in the H_2S conversion and S selectivity, which were attributed to the strengthened redox property due to the formation of the vanadium molybdate phase. In addition, Park et al. [145] examined the catalytic performance of vanadium-antimony mixed oxides (V-Sb-O/TiO_2). The addition of antimony led to the formation of the active $VSbO_4$ phase, which improved the regeneration of used V_2O_5/TiO_2 by providing spillover oxygen through the metal oxide boundary. Moreover, a study by Shin et al. [146] indicated that the activity of V_2O_5-TiO_2 was substantially improved when multiple metals such as Fe, Cr, and Mo were incorporated. This was attributed to the increased redox capability, especially in the re-oxidation stage. The regeneration of the reduced vanadium oxide corresponds to the rate-determining step, i.e., the step that determines the overall velocity of catalytic

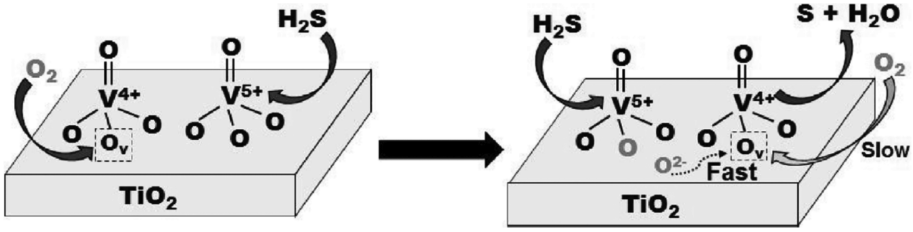

Fig. 3. Rapid re-oxidation of the reduced V_2O_5-TiO_2 catalyst by oxygen anions generated from nearby oxygen vacancies in selective oxidation of H_2S [1].

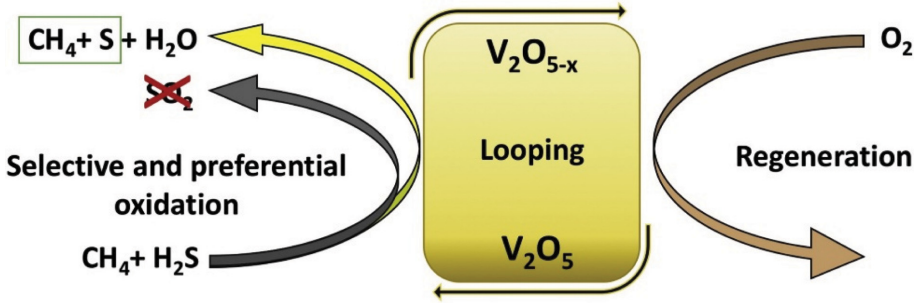

Fig. 4. Selective oxidation of H_2S and regeneration of the catalyst during the chemical looping process [147].

reaction [124]. The acceleration of the re-oxidation step in the presence of oxygen vacancy in V_2O_5-TiO_2 catalysts is explained schematically in Fig. 3. Recently, Phatyenchuen et al. [141] prepared transition metal (e.g., La, Zr, Nb, and Y)-doped V_2O_5/TiO_2 catalysts. The highest activity was found in the yttrium-doped catalyst due to the increased oxygen vacancies by the substitution of Y^{3+} cations for Ti^{4+} in the TiO_2 crystalline lattice. The effects of other dopants were less positive than that of Y due to their higher valence states (Nb^{5+} and Zr^{4+}) or larger ionic radii (Y^{3+}=0.80 Å and La^{3+}= 1.15 Å) compared to Ti^{4+}.

The chemical looping (CL) concept has recently been introduced to improve the selectivity of vanadium-based catalysts during H_2S oxidation [147,148]. Here, in contrast to general catalytic processes, the reactant gases are fed alternatively via fixed bed switching reactors. Bulk V_2O_5 or supported vanadium oxides as oxygen carriers are periodically reduced and oxidized by H_2S and O_2, respectively. Although this approach has not enabled the complete oxidation of H_2S during the reductant step, effective removal of deposited sulfur from the catalyst surfaces has been achieved during the oxidant step (Fig. 4). Hence, although the application of the CL concept to H_2S oxidation has shown potential for high selectivity towards the production of elemental sulfur, further studies are needed to raise the conversion ratio of H_2S in the reductant step.

2. Magnesium Oxide-based Catalysts

The mechanism of catalytic H_2S oxidation by magnesium oxide differs from that of vanadium oxide in that the pH value of the catalyst plays an important role, with the H_2S being adsorbed and dissociated into HS^- and H^+ on the alkaline surface of the catalyst [149]. The hydrosulfide anions are then oxidized to elemental sulfur by reactive oxygen radicals as follows [17]:

$$H_2S+OH^- \rightarrow HS^- +H^+ +OH^- \quad (11)$$

$$HS^- +H^+ +O^* \rightarrow H_2O+S \quad (12)$$

Because the dissociation of H_2S and the formation of oxygen radicals generally occur in the water film present on the catalyst surface, the catalytic performance is significantly influenced by the relative humidity (RH) [150]. It has been reported that catalytic reactions are activated at RH values of around 20%.

Magnesium oxide (MgO) is a suitable material for dissociating H_2S because its rich basic surface sites and partial solubility in water continuously provide OH^- [129]. In addition, surface modification with caustic chemicals (e.g., NaOH, Na_2CO_3, KOH) boosts the dissociation of H_2S, thus improving the catalytic activity [47, 151,152]. A recent study demonstrated the stable capability of H_2S conversion by MgO compared to other impregnated basic salts on mesoporous carbon, which was attributed to the stable release of OH^- without consumption by acid-base neutralization reactions between OH^- and H^+ (Fig. 5) [153].

Alternatively, Yang et al. [129] studied desulfurization by ZnO-MgO supported on activated carbon to indicate a satisfactory H_2S breakthrough capacity even under dry conditions, thus suggesting that the dissociation of H_2S by MgO is favored in the presence of a small quantity of adsorbed water. Furthermore, the XPS study indi-

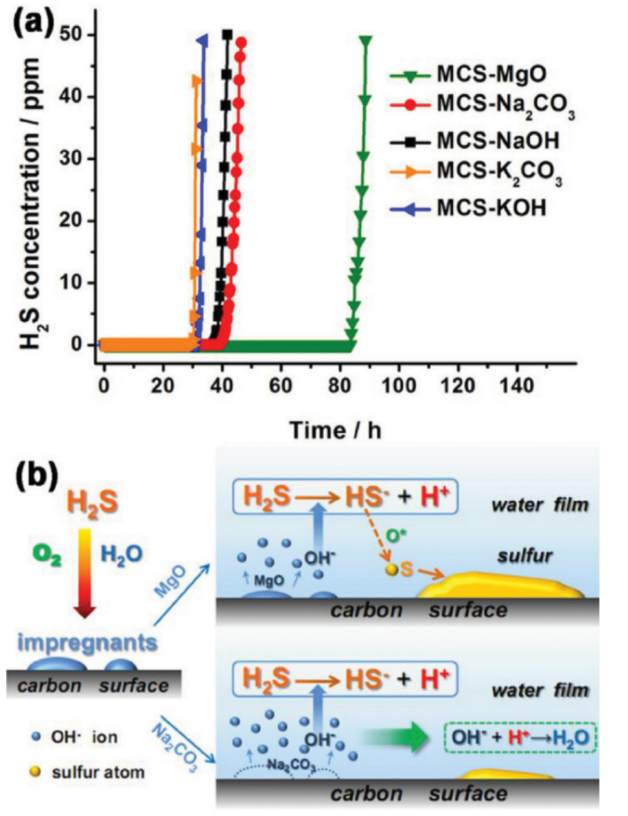

Fig. 5. (a) H_2S breakthrough curves over the catalysts with different caustic impregnants and (b) schematic illustration of the H_2S oxidation process over MCSs with MgO and soluble salts [153].

cated that the MgO was not consumed during desulfurization, thus demonstrating that the MgO takes part in catalytic reactions. Based on significant findings, the cited authors proposed plausible reaction mechanisms of H_2S removal in wet and dry environments, respectively. In wet environment, the MgO is hydroxylated due to the presence of a water film. The hydroxylated magnesium oxide dissociates the H_2S into HS^-, which then interacts with reactive oxygen species derived from adsorbed O_2 to form elemental sulfur. Sulfuric acid is generated by the reaction of S, O_2, and H_2O, which is eventually followed by the formation of magnesium sulfate. The relevant reaction equations are as follows:

$$MgO+H_2O\rightarrow Mg(OH)_2 \quad (13)$$

$$Mg(OH)_2+H_2S\rightarrow Mg(OH)^++HS^-+H_2O \quad (14)$$

$$HS^-+1/2O_2\rightarrow S+OH^- \quad (15)$$

$$Mg(OH)^++OH^-\rightarrow Mg(OH)_2 \quad (16)$$

$$S+3/2O_2+H_2O\rightarrow H_2SO_4 \quad (17)$$

$$H_2SO_4+Mg(OH)_2\rightarrow MgSO_4+2H_2O \quad (18)$$

In dry environment, the key difference is that Brønsted acid sites ($MgOH^+$) are generated on the MgO surface by capturing protons from H_2S in accordance with the following reaction [154,155]:

$$MgO+H_2S\rightarrow MgOH^++HS^- \quad (19)$$

This results in the dissociative adsorption of H_2S onto the MgO surface, which facilitates the formation of elemental sulfur via the reaction of HS^- and O_2 even under dry conditions.

Zhang et al. [156] conducted an interesting study on desulfurization using layered double hydroxides (LDH) composed of Mg, Al, and V. The LDH exhibited high H_2S removal performance with a maximum sulfur yield of 95% at 180 °C due to the combined effect of (i) the abundance of moderately basic sites on the MgO, where the H_2S is readily adsorbed to form S^{2-} and H_2O, and (ii) the uniform dispersion of pentavalent vanadium species (V^{5+}), which oxidize S^{2-} to elemental S with the formation of oxygen vacancy in Mg-O bonds. Although the consumption of the moderately basic sites leads to deactivation of the catalyst, the basic sites are recovered by incorporation of O^{2-} into the oxygen vacancies after oxidation of V^{4+} to V^{5+} by O_2. These processes are briefly expressed by the following equations:

$$Mg\text{-}O\text{-}Mg+H_2S\rightarrow Mg\text{-}S\text{-}Mg+H_2O \quad (20)$$

$$Mg\text{-}S\text{-}Mg+V^{5+}\rightarrow Mg\text{-}\square\text{-}Mg+V^{4+}+S \quad (21)$$

$$V^{4+}+Mg\text{-}\square\text{-}Mg+1/2O_2\rightarrow Mg\text{-}O\text{-}Mg+V^{5+} \quad (22)$$

3. Iron Oxide-based Catalysts

Conventionally, iron oxide-based catalysts have been used to treat the remaining H_2S in the Claus tail gas [157-160]. Although iron oxide is advantageous to H_2S oxidation in terms of its moisture resistance and relatively high conversion [161,162], major drawbacks include low selectivity towards sulfur production due to the requirement for excess oxygen and rapid deactivation during catalytic reactions [162]. These limitations have led to research on the modification of iron oxide with various metal oxides for improved selectivity and stability [139,159,163-165]. Chromium was first incorporated to produce mixed Fe-Cr oxides deposited on α-Al_2O_3 [157]. The Cr-modified catalysts were known to have several merits, including selectivity towards sulfur production and improved resistance to deactivation during desulfurization. Moreover, the addition of chromium increased the stability of the catalysts in a moisture-containing environment, which made the in-stream removal of water unnecessary [17]. Although there is no direct evidence, the improved performance of Cr-incorporated catalysts has been attributed to the presence of multivalent iron species (Fe(II)/Fe(III)) and iron sulfate as the active phase. Nevertheless, the sulfur yield remains unsatisfactory (80%) and the use of chromium can be a problem due to its toxicity. Hence, alternative catalysts such as Fe_2O_3 supported on silica have been developed and applied to H_2S oxidation. For instance, Terörde et al. [160] studied the catalytic performance of iron oxide-based catalysts with various supports to find that α-Al_2O_3-supported Fe_2O_3 catalyst exhibited the best activity, with a maximum sulfur selectivity of 94% at 247 °C in a feed gas composed of 1 vol% H_2S, 5 vol% O_2, 30 vol% H_2O with a balance of He. Catalyst deactivation was generally driven by deposition of iron(II) sulfates formed during the catalytic reactions, which prevented the reactants from being adsorbed onto the active sites. Although the use of SiO_2 resulted in excellent performance by effectively suppressing the sintering of $FeSO_4$, a steep decline in the sulfur selectivity was observed at higher temperature. This was assumed to be caused by the activated reaction between molecular oxygen and S radical on the silica support, but is also related to the formation of ferrous disulfide (FeS_2). The low selectivity problem was solved by the addition of 3 wt% sodium to give a high selectivity of >80% at 290 °C, compared to less than 50% in the absence of sodium [158]. The addition of sodium led to the formation of sodium sulfate on the silica support, thus suppressing the generation of strongly acidic sites so that sulfur radicals could not be formed due to the lack of Lewis acids to cleave the S-S bonds.

Bukhtiyarova et al. [163] studied the effect of calcination temperature upon the property of Fe_2O_3/SiO_2 catalysts to demonstrate increased stability against sulfidation, which is favorable to the extension of the catalyst lifespan, with increasing calcination temperature [163]. Nevertheless, agglomeration of the iron oxide particles was also observed at higher calcination temperature, thus resulting in lower concentration of active surface sites and, hence, reduced catalytic activity. Antimony and tin have also been incorporated to modify the catalytic performance of iron oxide [165]. Iron-antimonate and iron-tin catalysts with various compositions have been tested for H_2S oxidation with a H_2S/O_2 ratio of 1 : 5 at 200-280 °C. The catalytic activity was found to be substantially affected by the catalyst composition, with a 3 : 2 ratio of Fe to Sb giving the best H_2S conversion and S selectivity over the entire temperature range. However, catalysts with excess antimony displayed much lower activity than that of the pristine iron oxide. In particular, the performance of the various iron-tin catalysts was invariably superior to that of the single metal oxide, with Fe to Sn ratios of 1 : 7 and 2 : 9 giving the highest activity along with 100% conversion at 200 °C due to their high surface area. This perfect selectivity was maintained with the same atomic ratio of iron and

Table 6. Various metal oxide-based catalysts and these H_2S removal performances at specific reaction conditions

Catalyst	Feed gas	Temperature (°C)	Performance		Reference
			Conversion (%)	Selectivity (%)	
V-Sb-O/ZrO_2	H_2S: 1%, O_2: 5% (N_2 base)	180	95.4	100	[142]
V_2O_5/Y-TiO_2	H_2S: 300 ppm, O_2: 150 ppm, CH_4: 1%, CO_2: 1% (He base)	130	80	91	[141]
Na-promoted V_2O_5	H_2S: 1.2%, Air: 5% (He base)	200	98	100	[138]
Mo-V-O/TiO_2	H_2S: 5%, O_2: 2.5%, NH_3: 5%, H_2O: 60%, He: 27.5%	260	86	82.3	[144]
VO_x/SiO_2	H_2S: 5%, O_2: 2.5% (He balance)	225	98	99.1	[146]
Fe_2O_3-Cr_2O_3/α-Al_2O_3	H_2S: 1%, O_2: 5%, H_2O: 30%, He: 64%	292	95	91	[160]
Fe_2O_3/SiO_2	H_2S: 1%, O_2: 5%, H_2O: 30%, He: 64%	240	100	95	[158]
$FeSbO_4$	H_2S: 1%, O_2: 5% (He base)	210	100	100	[165]
Fe_2O_3/SiC	H_2S: 1%, O_2: 2.5%, H_2O: 30%, He: 66.5%	250	100	95	[164]
Fe/Ce	H_2S: 1%, O_2: 0.5% (He base)	250	100	99	[162]

tin in the temperature range of 240-300 °C. The improvement in the catalytic performance of mixed metal oxides is attributed to a remote-control mechanism [166] in which the Fe_2O_3 synergizes the effects of $FeSbO_4$ or SnO_2 via mobile oxygen species: oxygen molecules activated by the Fe sites in Fe_2O_3 migrate to the Sb or Sn sites in $FeSbO_4$ or SnO_2, where the oxidation of H_2S is facilitated by the creation of new active sites.

The decline in the selectivity for the production of elemental sulfur is related to the formation of hot spots on the catalyst surface due to the heat of the H_2S oxidation reaction, which could lead to a further reaction between sulfur and oxygen to form SO_2. This problem has been avoided by the use of silicon carbide (β-SiC) as a support material for the iron oxide-based catalyst [164], with the following advantages for desulfurization: (i) due to the strong interaction between the SiC and Fe_2O_3, the active Fe_2O_3 particles are evenly dispersed on the SiC surface with spacings of ~2-5 nm; (ii) the high thermal conductivity of the silicon carbide facilitates efficient heat dispersion into the catalyst bed; and (iii) the chemical inertness of SiC enables the catalyst to be used even under corrosive conditions with a H_2S concentration of 2.7%. These properties of the SiC-supported catalyst afford excellent catalytic activity of 100% conversion and 95% selectivity at 250 °C. Deactivation of the catalyst is also effectively restrained under a high H_2S concentration of 2.7% and a high reaction temperature of 250 °C, retaining a H_2S conversion of 97% and an S selectivity of 93%.

Although the rapid deactivation of iron-based catalysts is a serious issue, it can be relieved by providing the catalysts with excess oxygen from additive materials. In this regard, cerium oxide is a suitable candidate due to its high redox property and facile mobility of oxygen [167]. Koyuncu and Yasyerli studied the influence of cerium oxide on the selectivity and stability of Fe-Ce mixed oxide catalysts for H_2S oxidation [162]. Tests revealed that the catalyst with an Fe/Ce ratio of 1 : 1 exhibited notably improved stability against deactivation, retaining 100% H_2S conversion and 99% selectivity for sulfur at 300 °C with O_2/H_2S=0.5. This excellent catalytic performance is attributed to the enhanced redox property of the cerium-incorporated catalysts, such that additional oxygen is supplied to effectively suppress the deactivation driven by sulfidation on the iron oxide surface. The metal oxide-based catalysts introduced in this section are summarized, along with their major reaction conditions and catalytic performances, in Table 6.

STATE OF THE ART

The conventional technology stream has separately focused on desulfurization either by adsorption or catalytic oxidation. The adsorption process can effectively remove H_2S even at low temperature by capturing H_2S molecules in the pore structure or by chemically reacting H_2S with metal oxides. However, the desorption of adsorbed sulfur species without damaging the sorbent structures is a great challenge which should be overcome to enable the repetitive use of sorbents in the desulfurizer. Catalytic oxidation has the virtue of the direct and thermodynamically favorable selective oxidation of H_2S to elemental sulfur [17]. However, drawbacks include the low surface area of metal oxide-based catalysts and high-temperature requirements for catalytic reactions. Therefore, a combination of the two strategies would provide a breakthrough for H_2S removal performance by providing materials with dual functionality. The recent development of nanotechnology enables researchers to synthesize tailored nanoporous catalysts that could effectively remove H_2S even at room temperature due to the enhanced accessibility of adsorption sites. With this in mind, recent studies have demonstrated the syntheses of dual-functioning materials composed of highly dispersed metal oxide nanoparticles on AC supports [168,169]. For example, Yang et al. adopted a novel strategy for enhancing the H_2S uptake capacity by tuning the interaction between ZnO nanoparticles and the AC support via the introduction of nitrogen species on the AC surface [168]. The N-modified AC with ZnO exhibited a substantially improved H_2S removal performance with 66.4 mg-H_2S/g-sorbent at room temperature, which was much higher than that of ZnO-supported AC without nitrogen (32.4 mg-H_2S/g-sorbent). This clearly demonstrates the positive effect of nitrogen addition to the AC support for H_2S removal: the electron density of the ZnO is decreased due to the interaction between ZnO and the N-modified AC, thus resulting in the formation of defects such as grain boundaries or oxygen vacancies in the ZnO [170]. The increased utilization of ZnO was attributed to an accelerated rate of lattice diffusion in the presence

of these defects, as confirmed by the complete disappearance of the characteristic XRD peaks of ZnO. In addition, the introduced N species served as basic sites which strengthened the basicity of the water film present on the AC surface, thus facilitating the dissociation of H_2S into HS^- or S_2^-. These species are readily oxidized to elemental sulfur [171] or reacted with ZnO to form ZnS. Moreover, the superior capacity of the N-modified AC (25.7 mg-H_2S/g-sorbent) compared to that of the pristine AC (2.9 mg-H_2S/g-sorbent) suggests that catalytic oxidation of H_2S was activated by the introduction of N species [172]. The overall reaction mechanism of the N-modified, ZnO dispersed AC is schematically presented in Fig. 6.

Similarly, Cimino et al. investigated the H_2S removal mechanism of CuO and ZnO dispersed onto AC [169] to demonstrate a higher H_2S adsorption capacity in the presence of both metal oxides rather than only CuO or ZnO, which was attributed to a promoting effect of CuO as oxygen donor when H_2S is reacted with ZnO to form $ZnSO_4$ [43]. Interestingly, XPS analysis revealed that the CuO sites, contrary to ZnO, could also induce catalytic oxidation of H_2S to elemental sulfur in the presence of H_2O and O_2 [173, 174], thus resulting in significant improvement of the H_2S adsorption capacity. The catalytic oxidation could occur via two possible routes: (i) the HS^- species formed by dissociation of H_2S in the water film on the AC surface can be directly converted to sulfur over the CuO sites, and (ii) the copper sulfides or sulfates formed by reactive adsorption of H_2S could be restored to copper oxide by molecular oxygen [174,175].

A novel research trend has been to synthesize highly efficient

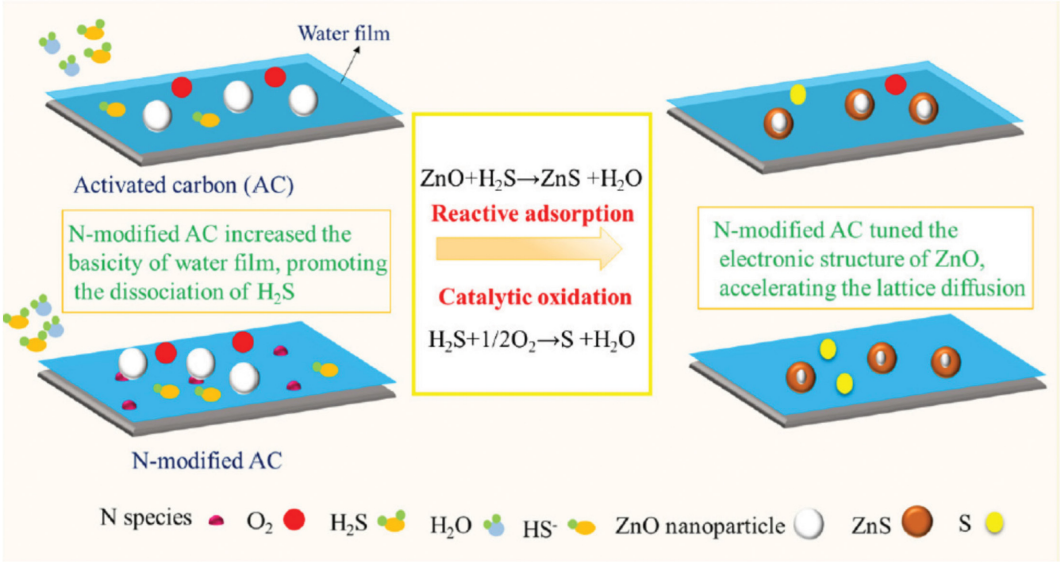

Fig. 6. Schematic diagram for the H_2S removal mechanism by both reactive adsorption and catalytic oxidation in ZnO-dispersed N-modified AC [168].

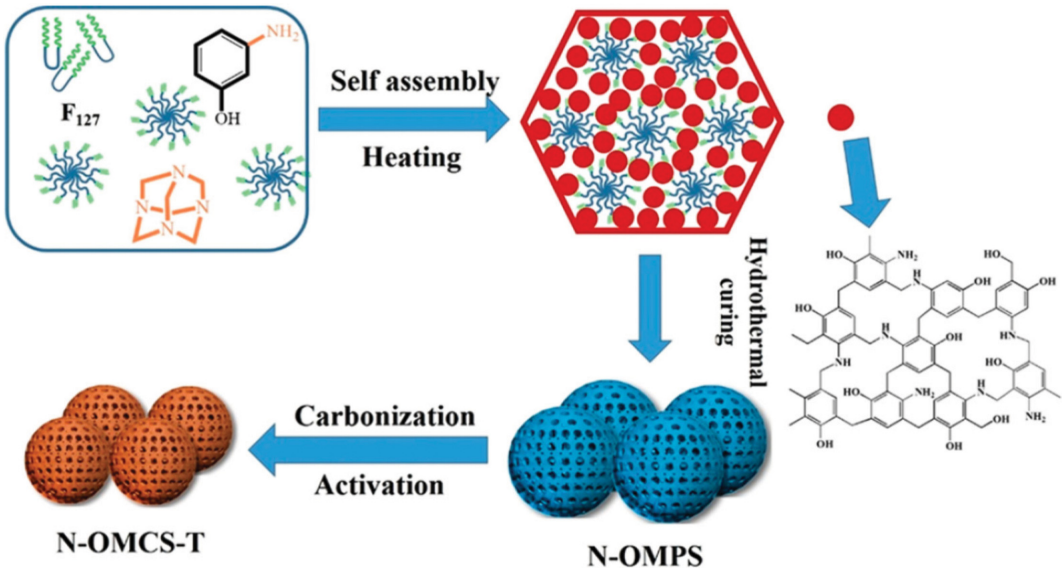

Fig. 7. Schematic diagram for the synthesis of N-OMCS-T [176].

metal-free catalysts based on carbon materials (e.g., carbon spheres [176] , carbon nanosheets [177], and graphene aerogel [178]) with excellent H_2S adsorption capacity due to the large BET surface area and porosity. For example, Kan et al. [176] explored the H_2S removal performance of a class of nitrogen-decorated ordered mesoporous carbon spheres (N-OMCS-T) that were prepared from a series of processes including the self-assembly of a block copolymer template, hydrothermal curing, and controlled carbonization followed by activation with KOH (Fig. 7). The synthesized N-OMCS-T exhibited a hierarchical pore structure with a large BET surface area together with controlled nitrogen functional groups, resulting in excellent selective H_2S capture (max. 457 mg/g, 0 °C and 1 bar) over CO_2, CH_4, and N_2. Moreover, the adsorbed H_2S was selectively oxidized to elemental sulfur in the temperature range of 100-120 °C. This work is meaningful in terms of the development of metal-free catalysts for H_2S oxidation, which generally have higher resistance to sulfur compared with metal-based catalysts [179,180]. However, these materials could not overcome the high-temperature requirements of the catalytic reaction. In this respect, it is desirable to synthesize metal-free catalysts that function even at room temperature. For example, Yu et al. reported a synthesis of nitrogen-doped mesoporous carbon nanosheets (NMCS) from Zn-based zeolitic imidazolate frameworks (ZIF-8) for use in desulfurization [177]. The detailed characterization revealed that the unique structure of the NMCS was formed by a salt templating pathway through which molten salts induce the generation of carbon nanosheets and the mesoporous structure during the carbonization process (Fig. 8). Due to its structural advantage, the NMCS exhibited a high breakthrough sulfur capacity of 0.54 g-H_2S/g-catalyst, whereas samples obtained by direct pyrolysis of ZIF-8 in the absence of salts showed very poor performance. In addition, the H_2S removal capacity was greatly enhanced to 1.46 g-H_2S/g-catalyst when the NMCS was impregnated with Na_2CO_3. The positive effect of Na_2CO_3 on the selective oxidation of H_2S has also been investigated [181-183] explaining that the addition of Na_2CO_3 increases the alkalinity of the material surfaces, thus facilitating the

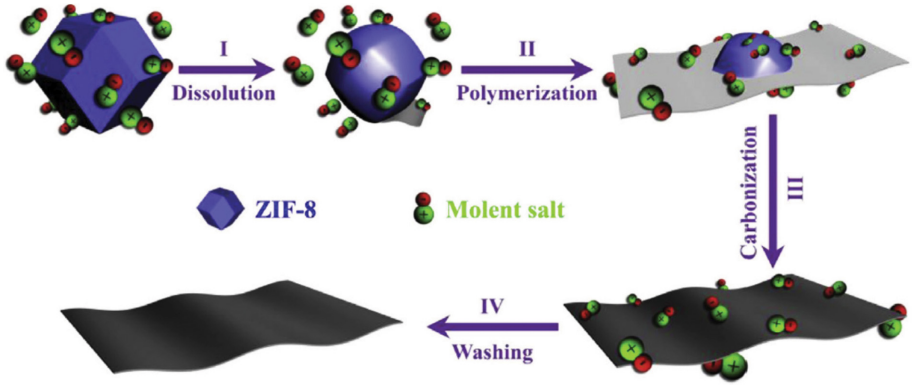

Fig. 8. Schematic diagram of the synthetic process for 2D N-doped mesoporous carbons nanosheets from microporous ZIF-8 polyhedrons in a molten salt medium [177].

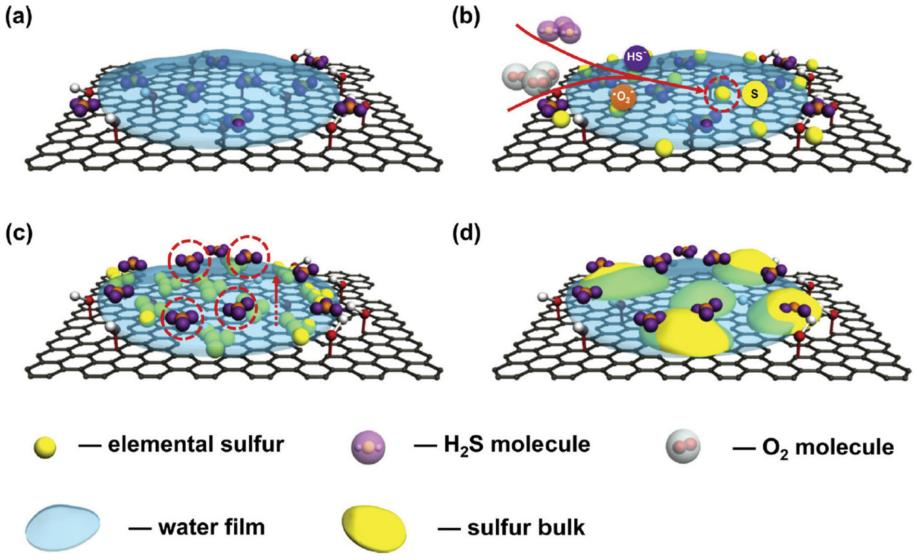

Fig. 9. Schematic illustration of the H_2S removal on the alkaline graphene aerogels: (a) The formation of water film; (b) schematic representation of the oxidation mechanism; (c) the process of deposition of sulfur product on graphene sheets; and (d) schematic diagram of the exhausted catalyst [178].

Table 7. Various metal-free, carbon-based catalysts studied in selective oxidation of H_2S to elemental sulfur at low temperatures.

Catalyst	Feed gas	Temperature (°C)	Breakthrough capacity (g-H_2S/g-catalyst)	Reference
Pitch-based activated carbon fibers	H_2S: 1,000 ppm, O_2: 1%, RH: 80%	30	0.75	[183]
Alkaline carbon nanotubes	H_2S: 1,000 ppm, O_2: 1%, RH: 80%	30	1.60	[182]
Carbon aerogels	H_2S: 1,000 ppm, O_2: 1%, RH: 80%	30	1.71	[182]
N-doped mesoporous carbons	H_2S: 1,000 ppm, O_2: 1%, RH: 80%	30	2.94	[177]
Mesoporous carbon spheres	H_2S: 1,000 ppm, O_2: 1%, RH: 80%	30	2.61	[153]
N-doped mesoporous carbon nanosheets	H_2S: 1,000 ppm, O_2: 2%, RH: 70%	25	1.46	[177]
Alkaline mesoporous carbons	H_2S: 1,000 ppm, O_2: 1%, RH: 80%	30	2.82	[184]
Alkaline graphene aerogel	H_2S: 1,000 ppm, O_2: 1%, RH: 80%	30	3.39	[178]

dissociation of H_2S into HS^-. In addition, Pan et al. [178] reported the synthesis of Na_2CO_3-impregnated graphene aerogels with an outstanding catalytic performance of 3.39 g-H_2S/g-catalyst at room temperature, which was attributed to the combined effect of the introduction of Na_2CO_3 and the interconnected graphene network (Fig. 9). The recent studies on carbon-based metal-free catalysts for selective low-temperature oxidation of H_2S are listed in Table 7.

CONCLUSIONS AND PERSPECTIVES

The control of hydrogen sulfide generated from landfills or chemical industries is a major issue due to its deleterious effect on the environment. To meet the strict environmental regulations, various technologies such as stripping, absorption, microbiological treatment, adsorption, and catalytic oxidation have been developed and applied in H_2S removal processes. Among these, adsorption and catalytic oxidation could be considered as promising for desulfurization in terms of their simplicity, efficiency, and economy.

Materials with high surface area and large pore volume, such as activated carbons (ACs), zeolites, mesoporous silica, and metal organic frameworks (MOFs), are generally adopted for the adsorption process. Moreover, since the H_2S removal performance of an adsorbent is closely related to its surface property, the above materials are frequently functionalized to improve their H_2S sorption capacity. For the ACs, the influence of surface basicity has been investigated by several research groups to indicate that the increased surface alkalinity in the presence of amine functional groups is beneficial for H_2S adsorption. Several studies on the recyclability of ACs have indicated that H_2S adsorption is inherently irreversible, which seriously limits the commercial application of ACs for desulfurization. Zeolites are usually modified with various metal cations by ion exchange or wet impregnation for H_2S removal. The improvement of H_2S removal performance by modification with metal cations is considered to involve the following two factors: (i) the enhanced diffusion of H_2S molecules into zeolite cavities, and (ii) the strong affinity of metal cations for sulfur anions. Nevertheless, the reported H_2S adsorption capacity of zeolite-type adsorbents is relatively low compared to those of other porous sorbents, probably because the microporous zeolite structure limits the efficient diffusion of H_2S molecules into the inner cavities.

Similarly to ACs, various mesoporous silicas modified with amine functional groups have been used for H_2S removal. Although the application of mesoporous silicas for desulfurization seems reasonable in terms of adsorption performance and regeneration, the synthetic processes of these materials should be further studied to reduce the production cost that presently inhibits their mass-production for full-scale applications. Meanwhile, the application of MOFs for desulfurization is considered as a possible alternative to conventional porous sorbents such as ACs, zeolites, or mesoporous silicas since various functionalities can be provided by tailored design. Despite a few encouraging results showing superior performance and regenerability, insufficient data have been accumulated to fully appraise their applicability to H_2S removal processes; hence, a consistent range of studies on the use of MOFs needs to be conducted.

The catalytic oxidation process removes H_2S by selective oxidation to elemental sulfur at moderately elevated temperature. Hence, metal oxide-based catalysts (e.g., VO_x, MgO_x, FeO_x) have been investigated. The activity of vanadium oxide-containing catalysts largely depends on the presence of V_4O_9, which leads to the formation of oxygen vacancies and enhanced redox property. The effects of various supports or the modification of metal oxides have been actively studied. The improved performance is closely related to the increased ratio of V^{4+}/V^{5+} resulting from the interaction between V_2O_5 and dopant metals or supports. Magnesium oxide can boost the rate of catalytic reactions by raising the alkalinity of the catalysts, which is favorable for the generation of reactive HS^- anions from H_2S. Iron oxide, conventionally used to control H_2S in the Claus tail gas, has the advantage of strong moisture resistance and high performance of H_2S removal. However, low selectivity towards the production of sulfur, along with fast deactivation, are disadvantages. Therefore, metal-modified iron oxide catalysts have been investigated to increase the feasibility of iron oxide-based catalysts in desulfurizing processes. Although metal oxide-based catalysts have shown impressive performance in H_2S removal, the surface areas of metal oxides and the working temperatures in catalytic oxidation are not comparable to those of the adsorption process.

A combination of the two key technologies (adsorption and catalytic oxidation) could overcome the limitations of current methods and open a new era of desulfurization. In this sense, the latest research into dual-functioning materials is worthy of notice. One approach is to synthesize sorbents composed of porous materials in which metal oxide nanoparticles are highly dispersed. This leads to improvement of the H_2S removal performance due to the high utilization of active materials. Another strategy involves metal-free

catalysts based on porous carbons, where a few studies have reported catalytic reactions even at room temperature. This is encouraging in terms of reducing the operational cost of commercial H_2S removal processes. It is expected that continuous efforts to investigate the performance of catalysts under various synthesis and operation conditions would lead to the development of an optimized technology for desulfurization.

ACKNOWLEDGEMENTS

This work was supported by the National Research Foundation of Korea (NRF) grant funded by the Korea government (MSIT) (No. NRF-2018R1C1B5085444), Korea Ministry of Environment (MOE) as Waste to energy recycling Human resource development Project, and the Daejeon Green Environment Center under the Research Development Program (Yr 2019) and the author would like to acknowledge for the assistance.

REFERENCES

1. B. Pongthawornsakun, S. Phatyenchuen, J. Panpranot and P. Praserthdam, *J. Environ. Chem. Eng.*, **6**, 1414 (2018).
2. O. A. Habeeb, R. Kanthasamy, G. A. M. Ali, S. Sethupathi and R. B. M. Yunus, *Rev. Chem. Eng.*, **34**, 837 (2018).
3. L. Skrtic, Hydrogen Sulfide, Oil and Gas, and People's Health, Master's Thesis (2006).
4. C. Selene and J. Chou, *Hydrogen sulfide: human health aspects*, World Health Organization, The Ohio State University (2003).
5. T. L. Guidotti, *Int. Arch. Occ. Env. Hea.*, **66**, 153 (1994).
6. J. Vollertsen, A. H. Nielsen, H. S. Jensen, T. Wium-Andersen and T. Hvitved-Jacobsen, *Sci. Total Environ.*, **394**, 162 (2008).
7. V. Garcia-Arriaga, J. Alvarez-Ramirez, M. Amaya and E. Sosa, *Corrosion Sci.*, **52**, 2268 (2010).
8. D. A. Dohnalek and J. A. FitzPatrick, *J. Am. Water Works Assn.*, **75**, 298 (1983).
9. M. H. Almasvandi, M. Rahimi and Y. Tagheie, *J. Nat. Gas Sci. Eng.*, **34**, 499 (2016).
10. C.-C. Lien, J.-L. Lin and C.-H. Ting, *J. Agric. Chem. Environ.*, **03**, 1 (2014).
11. R. A. S. Lestari, W. B. Sediawan, S. Syamsiah, Sarto and J. A. Teixeira, *J. Environ. Chem. Eng.*, **4**, 2370 (2016).
12. K. Sakanishi, Z. Wu, A. Matsumura, I. Saito, T. Hanaoka, T. Mowa, M. Tada and T. Iwasaki, *Catal. Today*, **104**, 94 (2005).
13. E. Laperdrix, G. Costent, N. Nguyen, F. Studer and J. C. Lavalley, *Catal. Today*, **61**, 149 (2000).
14. M. Khabazipour and M. Anbia, *Ind. Eng. Chem. Res.*, **58**, 22133 (2019).
15. W. Ahmad, S. Sethupathi, G. Kanadasan, L. C. Lau and R. Kanthasamy, *Rev. Chem. Eng.*, In press (2019).
16. M. S. Shah, M. Tsapatsis and J. I. Siepmann, *Chem. Rev.*, **117**, 9755 (2017).
17. X. Zhang, Y. Tang, S. Qu, J. Da and Z. Hao, *ACS Catal.*, **5**, 1053 (2015).
18. D. Liu, Q. Wang, J. Wu and Y. Liu, *Environ. Chem. Lett.*, **17**, 259 (2019).
19. J. H. Ko, Q. Xu and Y. C. Jang, *Crit. Rev. Environ. Sci. Technol.*, **45**, 2043 (2015).
20. A. Peluso, N. Gargiulo, P. Aprea, F. Pepe and D. Caputo, *Sep. Purif. Rev.*, **48**, 78 (2019).
21. A. D. Wiheeb, I. K. Shamsud, M. A. Ahmad, M. N. Murat, J. Kim and M. R. Othman, *Rev. Chem. Eng.*, **29**, 449 (2013).
22. J. R. Li, R. J. Kuppler and H. C. Zhou, *Chem. Soc. Rev.*, **38**, 1477 (2009).
23. O. A. Habeeb, K. Ramesh, A. M. Gomaa, R. M. Ali, T. K. Yunus, O. A. Thanusha, M. Olalere, G. A. M. Ali, R. M. Yunus, T. K. Thanusha and O. A. Olalere, *Aust. J. Basic & Appl. Sci.*, **10**, 136 (2016).
24. T. J. Bandosz, *J. Colloid Interface Sci.*, **246**, 1 (2002).
25. A. Bagreev, F. Adib and T. J. Bandosz, *Carbon*, **39**, 1897 (2001).
26. M. Liang, C. Zhang and H. Zheng, *Adsorption*, **20**, 525 (2014).
27. F. Adib, A. Bagreev and T. J. Bandosz, *Environ. Sci. Technol.*, **34**, 686 (2000).
28. F. Adib, A. Bagreev and T. J. Bandosz, *J. Colloid Interface Sci.*, **216**, 360 (1999).
29. H. Förster and M. Schuldt, *J. Colloid Interface Sci.*, **52**, 380 (1975).
30. H. G. Karge and J. Raskó, *J. Colloid Interface Sci.*, **64**, 522 (1978).
31. G. Huang, E. He, Z. Wang, H. Fan, J. Shangguan, E. Croiset and Z. Chen, *Ind. Eng. Chem. Res.*, **54**, 8469 (2015).
32. E. Barea, C. Montoro and J. A. R. Navarro, *Chem. Soc. Rev.*, **43**, 5419 (2014).
33. J. B. Decoste and G. W. Peterson, *Chem. Rev.*, **114**, 5695 (2014).
34. K. Vellgiri, A. Deep and K. H. Kim, *ACS Appl. Mater. Interfaces*, **8**, 29835 (2016).
35. I. Ahmed and S. H. Jhung, *J. Hazard. Mater.*, **301**, 259 (2016).
36. C. Fauteux-Lefebvre, N. Abatzoglou, S. Blais, N. Braidy and Y. Hu, *Carbon*, **95**, 794 (2015).
37. C. Lin, W. Qin and C. Dong, *Appl. Surf. Sci.*, **387**, 720 (2016).
38. A. R. Barron, C. E. Coker and J. R. Loscutova, US Patent, 7,569,199 (2009).
39. J. Wang, L. Wang, H. Fan, H. Wang, Y. Hu and Z. Wang, *Fuel*, **209**, 329 (2017).
40. H. F. Garces, H. M. Galdo, L. J. Garces, J. Hunt, A. Morey and S. L. Suib, *Micropor. Mesopor. Mater.*, **127**, 190 (2010).
41. K. Ling, V. S. Gangoli and A. R. Barron, *Energy Fuels*, **33**, 7509 (2019).
42. D. A. Giannakoudakis and T. J. Bandosz, *J. Colloid Interface Sci.*, **436**, 296 (2014).
43. G. de Falco, F. Montagnaro, M. Balsamo, A. Erto, F. A. Deorsola, L. Lisi and S. Cimo, *Micropor. Mesopor. Mater.*, **257**, 135 (2018).
44. M. Florent, R. Wallace and T. J. Bandosz, *J. Colloid Interface Sci.*, **448**, 573 (2015).
45. A. Bagreev and T. J. Bandosz, *Ind. Eng. Chem. Res.*, **44**, 530 (2005).
46. M. C. Castrillon, K. O. Moura, C. A. Alves, M. Bastos-Neto, D. C. S. Azevedo, J. Hmann, J. Möllmer, W. D. Eicke and R. Gläser, *Energy Fuels*, **30**, 9596 (2016).
47. J. H. Tsai, F. T. Jeng and H. L. Chiang, *Adsorption*, **7**, 357 (2001).
48. A. Turk, E. Sakalis, J. Lessuck, H. Karamitsos and O. Rago, *Environ. Sci. Technol.*, **23**, 1242 (1989).
49. A. Turk, E. Sakalis, O. Rago and H. Karamitsos, *Ann. N. Y. Acad. Sci.*, **661**, 221 (1992).
50. J. P. Boudou, M. Chehimi, E. Broniek, T. Siemieniewska and J. Bimer, *Carbon*, **41**, 1999 (2003).
51. R. Sitthikhankaew, S. Predapitakkun, R. Kiattikomol, S. Pumhiran, S. Assabumrungrat and N. Laosiripojana, *Energy Procedia*, **9**,

15 (2011).
52. S. Bashkova, A. Bagreev and T.J. Bandosz, *Ind. Eng. Chem. Res.*, **41**, 4346 (2002).
53. A. Bagreev, F. Adib and T. J. Bandosz, *J. Colloid Interface Sci.*, **219**, 327 (1999).
54. T. J. Bandosz, *Carbon*, **37**, 483 (1999).
55. F. Adib, A. Bagreev and T. J. Bandosz, *Langmuir*, **16**, 1980 (2000).
56. S. Tian, H. Mo, R. Zhang, P. Ng and T. Zhou, *Adsorption*, **15**, 477 (2009).
57. A. Bagreev, H. Rahman and T. J. Bandosz, *Environ. Sci. Technol.*, **34**, 4587 (2000).
58. C. Fauteux-Lefebvre, N. Abatzoglou, N. Braidy and Y. Hu, *Ind. Eng. Chem. Res.*, **54**, 9230 (2015).
59. J. Zhang, L. Wang, H. Song and H. Song, *Res. Chem. Intermed.*, **41**, 6087 (2015).
60. M. Balsamo, S. Cimo, G. de Falco, A. Erto and L. Lisi, *Chem. Eng. J.*, **304**, 399 (2016).
61. Z. Qiao, Z. Wang, C. Zhang, S. Yuan, Y. Zhu and J. Wang, *AIChE J.*, **59**, 215 (2012).
62. D. W. Breck, *Zeolite molecular sieves: structure, chemistry, and use*, Wiley, New York (1974).
63. R. M. Barrer, *Zeolites and clay minerals as sorbents and molecular sieves*, Academic Press, London (1978).
64. A. J. Cramer and J. M. Cole, *J. Mater. Chem. A*, **5**, 10746 (2017).
65. D. Caputo, F. Iucolano, F. Pepe and C. Colella, *Micropor. Mesopor. Mater.*, **105**, 260 (2007).
66. D. M. Ruthven, *Principles of adsorption and adsorption processes*, Wiley, New York (1984).
67. D. Zhao, K. Cleare, C. Oliver, C. Ingram, D. Cook, R. Szostak and L. Kevan, *Micropor. Mesopor. Mater.*, **21**, 371 (1998).
68. M. Younas, M. Sohail, L. L. Kong, M. J. K. Bashir and S. Sethupathi, *Int. J. Environ. Sci. Technol.*, **13**, 1839 (2016).
69. C. L. Garcia and J. A. Lercher, *J. Phys. Chem.*, **96**, 2230 (1992).
70. P. Cosoli, M. Ferrone, S. Pricl and M. Fermeglia, *Chem. Eng. J.*, **145**, 86 (2008).
71. P. Cosoli, M. Ferrone, S. Pricl and M. Fermeglia, *Chem. Eng. J.*, **145**, 93 (2008).
72. C.-Y. Sung, S. Al Hashimi, A. McCormick, M. Cococcioni and M. Tsapatsis, *Micropor. Mesopor. Mater.*, **172**, 7 (2013).
73. L. Micoli, G. Bagnasco and M. Turco, *Int. J. Hydrogen Energy*, **39**, 1783 (2014).
74. I. N. Pavlova, R. S. Ilibaev, O. S. Travka and B. I. Kutepov, *Pet. Chem.*, **53**, 102 (2013).
75. P. Kumar, C.-Y. Sung, O. Muraza, M. Cococcioni, S. Al Hashimi, A. McCormick and M. Tsapatsis, *Micropor. Mesopor. Mater.*, **146**, 127 (2011).
76. M. M. Dubinin, M. A. Dzhcharadze, L. I. Efimova and A. A. Isirikyan, *Russ. Chem. Bull.*, **25**, 1820 (1976).
77. C. T. Kresge, M. E. Leonowicz, W. J. Roth, J. C. Vartuli and J. S. Beck, *Nature*, **359**, 710 (1992).
78. D. Zhao, *Science*, **279**, 548 (1998).
79. S. Ruthste, J. Schmidt, E. Kesselman, R. Popovitz-Biro, L. Omer, V. Frydman, Y. Talmon and D. Goldfarb, *Chem. Mater.*, **20**, 2779 (2008).
80. S. Che, A. E. Garcia-Bennett, T. Yokoi, K. Sakamoto, H. Kunieda, O. Terasaki and T. Tatsumi, *Nature Mater.*, **2**, 801 (2003).
81. D. Montes, E. Tocuyo, E. González, D. Rodríguez, R. Solano, R. Atencio, M. A. Ramos and A. Moronta, *Micropor. Mesopor. Mater.*, **168**, 111 (2013).
82. S. Inagaki, *Bull. Chem. Soc. Jpn.*, **69**, 149 (1996).
83. A. Andrzejewska, A. Krysztafkiewicz and T. Jesionowski, *Dyes Pigm.*, **75**, 116 (2007).
84. N. Gargiulo, F. Pepe and D. Caputo, *J. Nanosci. Nanotechnol.*, **14**, 1811 (2014).
85. N. Gargiulo, I. Attianese, G. G. Buonocore, D. Caputo, M. Lavorgna, G. Mensitieri and M. Lavorgna, *Micropor. Mesopor. Mater.*, **167**, 10 (2013).
86. H. Y. Huang, R. T. Yang, D. Chn and C. L. Munson, *Ind. Eng. Chem. Res.*, **42**, 2427 (2003).
87. X. Xu, I. Novochinskii and C. Song, *Energy Fuels*, **19**, 2214 (2005).
88. Q. Chen, F. Fan, D. Long, X. Liu, X. Liang, W. Qiao and L. Ling, *Ind. Eng. Chem. Res.*, **49**, 11408 (2010).
89. X. Wang, X. Ma, X. Xu, L. Sun and C. Song, *Top. Catal.*, **49**, 108 (2008).
90. X. Wang, T. Sun, J. Yang, L. Zhao and J. Jia, *Chem. Eng. J.*, **142**, 48 (2008).
91. Z. Ozayd, S. Yasyerli and G. Dogu, *Ind. Eng. Chem. Res.*, **47**, 1035 (2008).
92. J. L. C. Rowsell and O. M. Yaghi, *Micropor. Mesopor. Mater.*, **73**, 3 (2004).
93. M. Eddaoudi, J. Kim, N. Rosi, D. Vodak, J. Wachter, M. O'Keeffe and O. M. Yaghi, *Science*, **295**, 469 (2002).
94. M. Latroche, S. Surblé, C. Serre, C. Mellot-Draznieks, P. L. Llewellyn, J. H. Lee, J. S. Chang, S. H. Jhung and G. Férey, *Angew. Chem. Int. Ed.*, **45**, 8227, (2006).
95. A. G. Wong-Foy, A. J. Matzger and O. M. Yaghi, *J. Am. Chem. Soc.*, **128**, 3494 (2006).
96. S. Bourrelly, P. L. Llewellyn, C. Serre, F. Millange, T. Loiseau and G. Férey, *J. Am. Chem. Soc.*, **127**, 13519 (2005).
97. A. R. Millward and O. M. Yaghi, *J. Am. Chem. Soc.*, **127**, 17998 (2005).
98. K. Seki and W. Mori, *J. Phys. Chem. B*, **106**, 1380 (2002).
99. I. Ahmed and S. H. Jhung, *J. Hazard. Mater.*, **301**, 259 (2016).
100. K. Vellgiri, A. Deep and K.-H. Kim, *ACS Appl. Mater. Interfaces*, **8**, 29835 (2016).
101. E. Barea, C. Montoro and J. A. R. Navarro, *Chem. Soc. Rev.*, **43**, 5419 (2014).
102. J. B. DeCoste and G. W. Peterson, *Chem. Rev.*, **114**, 5695 (2014).
103. L. Hamon, C. Serre, T. Devic, T. Loiseau, F. Millange, G. Férey and G. D. Weireld, *J. Am. Chem. Soc.*, **131**, 8775 (2009).
104. A. Peluso, N. Gargiulo, P. Aprea, F. Pepe and D. Caputo, *Sci. Adv. Mater.*, **6**, 164 (2014).
105. X.-L. Wang, H.-L. Fan, Z. Tian, E.-Y. He, Y. Li and J. Shangguan, *Appl. Surf. Sci.*, **289**, 107 (2014).
106. S. Vaesen, V. Guillerm, Q. Yang, A. D. Wiersum, B. Marszalek, B. Gil, A. Vimont, M. Daturi, T. Devic, P. L. Llewellyn, C. Serre, G. Maur and G. De Weireld, *Chem. Commun.*, **49**, 10082 (2013).
107. Y. Li, L.-J. Wang, H.-L. Fan, J. Shangguan, H. Wang and J. Mi, *Energy Fuels*, **29**, 298 (2015).
108. P. K. Allan, P. S. Wheatley, D. Aldous, M. I. Mohideen, C. Tang, J. A. Hriljac, I. L. Megson, K. W. Chapman, G. D. Weireld, S. Vaesen and R. E. Morris, *Dalton Trans.*, **41**, 4060 (2012).

109. Y. Belmabkhout, R. S. Pillai, D. Alezi, O. Shekhah, P. M. Bhatt, Z. Chen, K. Adil, S. Vaesen, G. D. Weireld, M. Pang, M. Suet, A. J. Cairns, V. Solovyeva, A. Shkurenko, O. E. Tall, G. Maur and M. Eddaoudi, *J. Mater. Chem. A*, **5**, 3293 (2017).
110. H. H. Gunardson, *Industrial gases in petrochemical processing: chemical industries*, CRC Press, New York (1997).
111. X.-C. Huang, Y.-Y. Lin, J.-P. Zhang and X.-M. Chen, *Angew. Chem. Int. Ed.*, **118**, 1587 (2006).
112. Y. Liu, Y. Ma, Y. Zhao, X. Sun, F. Gándara, H. Furukawa, Z. Liu, H. Zhu, C. Zhu, K. Suenaga, P. Oleynikov, A. S. Alshammari, X. Zhang, O. Terasaki and O. M. Yaghi, *Science*, **351**, 365 (2016).
113. T. Ben, H. Ren, S. Ma, D. Cao, J. Lan, X. Jg, W. Wang, J. Xu, F. Deng, J. M. Simmons, S. Qiu and G. Zhu, *Angew. Chem. Int. Ed.*, **48**, 9457 (2009).
114. B. G. Goar, *Sulfur recovery technology*, CONF-860447, USA (1986).
115. E. Laperdrix, A. Sahibed-De, G. Costent, M. Bensitel and J. C. Lavalley, *Appl. Catal. B: Environ.*, **27**, 137 (2000).
116. K. A. Hawboldt, W. D. Monnery and W. Y. Svrcek, *Chem. Eng. Sci.*, **55**, 957 (2000).
117. W. D. Monnery, K. A. Hawboldt, A. Pollock and W. Y. Svrcek, *Chem. Eng. Sci.*, **55**, 5141 (2000).
118. M. Sassi and A. K. Gupta, *Am. J. Environ. Sci.*, **4**, 502 (2008).
119. J. S. Eow, *Environ. Progr.*, **21**, 143 (2002).
120. L. Ruiz-Rodríguez, T. Blasco, E. Rodríguez-Castellón and J. M. L. Nieto, *Catal. Today*, **333**, 237 (2019).
121. V. Palma and D. Barba, *Fuel*, **135**, 99 (2014).
122. V. Palma, D. Barba and V. Gerardi, *J. Clean. Prod.*, **111**, 69 (2016).
123. V. Palma and D. Barba, *Int. J. Hydrogen Energy*, **42**, 1891 (2017).
124. M. Y. Shin, D. W. Park and J. S. Chung, *Catal. Today*, **63**, 405 (2000).
125. L. Shen, X. Zheng, G. Lei, X. Li, Y. Cao and L. Jiang, *Chem. Eng. J.*, **346**, 238 (2018).
126. D. W. Park, S. W. Chun, J. Y. Jang, H. S. Kim, H. C. Woo and J. S. Chung, *Catal. Today*, **44**, 73 (1998).
127. D. Barba, V. Palma and P. Ciambelli, *Int. J. Hydrogen Energy*, **38**, 328 (2013).
128. M. D. Soriano, A. Vidal-Moya, E. Rodríguez-Castellón, F. V. Melo, M. T. Blasco and J. M. L. Nieto, *Catal. Today*, **259**, 237 (2016).
129. C. Yang, Y. Wang, H. Fan, G. de Falco, S. Yang, J. Shangguan and T. J. Bandosz, *Appl. Catal. B: Environ.*, **266**, 118674 (2020).
130. A. D. Wiheeb, I. K. Shamsud, M. A. Ahmad, M. N. Murat, J. Kim and M. R. Othman, *Rev. Chem. Eng.*, **29**, 449 (2013).
131. M. D. Soriano, J. A. Cecilia, A. Natoli, J. Jiménez-Jiménez, J. M. López Nieto and E. Rodríguez-Castellón, *Catal. Today*, **254**, 36 (2015).
132. K. V. Beesh, D. R. Cho, S. Y. Kim, B. R. Jermy and D. W. Park, *Catal. Commun.*, **9**, 2040 (2008).
133. M. I. Kim, W. D. Ju, K. H. Kim, D. W. Park and S. S. Hong, *Stud. Surf. Sci. Catal.*, **159**, 225 (2006).
134. M. D. Soriano, J. Jiménez-Jiménez, P. Concepción, A. Jiménez-López, E. Rodríguez-Castellón and J. M. L. Nieto, *Appl. Catal. B: Environ.*, **92**, 271 (2009).
135. J. P. Holgado, M. D. Soriano, J. Jiménez-Jiménez, P. Concepción, A. Jiménez-López, A. Caballero, E. Rodríguez-Castellón and J. M. L. Nieto, *Catal. Today*, **155**, 296 (2010).
136. M. D. Soriano, E. Rodríguez-Castellón, E. García-González and J. M. López Nieto, *Catal. Today*, **238**, 62 (2014).
137. W. Taifan and J. Baltrusaitis, *Catal. Sci. Technol.*, **7**, 2919 (2017).
138. M. D. Soriano, J. M. López Nieto, F. Ivars, P. Concepción and E. Rodríguez-Castellón, *Catal. Today*, **192**, 28 (2012).
139. A. A. Davydov, V. I. Marshneva and M. L. Shepotko, *Appl. Catal. A: Gen.*, **244**, 93 (2003).
140. T. Machej, J. Haber, A. M. Turek and I. E. Wachs, *Appl. Catal.*, **70**, 115 (1991).
141. S. Phatyenchuen, B. Pongthawornsakun, J. Panpranot and P. Praserthdam, *J. Environ. Chem. Eng.*, **6**, 5655 (2018).
142. K. T. Li and T. Y. Chien, *Catal. Lett.*, **57**, 77 (1999).
143. Z. Fan, H. Guo, K. Fang and Y. Sun, *RSC Adv.*, **5**, 24795 (2015).
144. B. G. Kim, W. D. Ju, I. Kim, H. C. Woo and D. W. Park, *Solid State Ion.*, **172**, 135 (2004).
145. D. W. Park, B. K. Park, D. K. Park and H. C. Woo, *Appl. Catal. A: Gen.*, **223**, 215 (2002).
146. M. Y. Shin, D. W. Park and J. S. Chung, *Appl. Catal. B: Environ.*, **30**, 409 (2001).
147. T. Kane, J. Guerrero-Caballero and A. Löfberg, *Appl. Catal. B: Environ.*, **265**, 118566 (2020).
148. D. Benvenuto, M. Giovannetti, A. Ciccozzi, S. Spoto, S. Angeletti and M. Ciccozzi, *J. Med. Virol.*, **92**, 455 (2020).
149. A. Bouzaza, A. Laplanche and S. Marsteau, *Chemosphere*, **54**, 481 (2004).
150. A. Primavera, A. Trovarelli, P. Andreussi and G. Dolcetti, *Appl. Catal. A: Gen.*, **173**, 185 (1998).
151. H. L. Chiang, J. H. Tsai, C. L. Tsai and Y. C. Hsu, *Sep. Sci. Technol.*, **35**, 903 (2000).
152. K. D. Henng and S. Schäfer, *Gas Sep. Purif.*, **7**, 235 (1993).
153. Z. Zhang, J. Wang, W. Li, M. Wang, W. Qiao, D. Long and L. Ling, *Carbon*, **96**, 608 (2016).
154. A. Travert, O. V. Manoilova, A. A. Tsyganenko, F. Maugé and J. C. Lavalley, *J. Phys. Chem. B*, **106**, 1350 (2002).
155. L. Oliviero, H. Leclerc, O. V. Manoilova, V. Blas-Aube, F. Maugé, E. V. Kondratieva, M. S. Poretsky and A. A. Tsyganenko, *Ind. Eng. Chem. Res.*, **48**, 1237 (2009).
156. X. Zhang, Z. Wang, N. Qiao, S. Qu and Z. Hao, *ACS Catal.*, **4**, 1500 (2014).
157. P. F. M. T. van Nisselrooya and J. A. Lagasb, *Catal. Today*, **16**, 263 (1993).
158. R. J. A. M. Terörde, M. C. de Jong, M. J. D. Crombag, P. J. van den Brk, A. J. van Dillen and J. W. Geus, *Stud. Surf. Sci. Catal.*, **82**, 861 (1994).
159. E. Laperdrix, G. Costent, N. N. Guyen, O. Saur and J. C. Lavalley, *J. Catal.*, **187**, 385 (1999).
160. R. J. A. M. Terörde, P. J. van den Brink, L. M. Visser, A. J. van Dillen and J. W. Geus, *Catal. Today*, **17**, 217 (1993).
161. J. H. Uhm, M. Y. Sh, J. Zhidong and J. S. Chung, *Appl. Catal. B: Environ.*, **22**, 293 (1999).
162. D. D. E. Koyuncu and S. Yasyerli, *Ind. Eng. Chem. Res.*, **48**, 5223 (2009).
163. G. A. Bukhtiyarova, V. I. Bukhtiyarov, N. S. Sakaeva, V. V. Kaichev and B. P. Zolotovskii, *J. Mol. Catal. A: Chem.*, **158**, 251 (2000).
164. P. Nguyen, D. Edouard, J. M. Nhut, M. J. Ledoux, C. Pham and

C. Pham-Huu, *Appl. Catal. B: Environ.*, **76**, 300 (2007).
165. K. T. Li, C. S. Yen and N. S. Shyu, *Appl. Catal. A: Gen.*, **156**, 117 (1997).
166. L. T. Weng, P. Patrono, E. Sham, P. Ruiz and B. Delmon, *J. Catal.*, **132**, 360 (1991).
167. S. Matsumoto, *Catal. Today*, **90**, 183 (2004).
168. C. Yang, S. Yang, H. Fan, Y. Wang and J. Shangguan, *J. Colloid Interface Sci.*, **555**, 548 (2019).
169. S. Cimo, L. Lisi, A. Erto, F. A. Deorsola, G. de Falco, F. Montagnaro and M. Balsamo, *Micropor. Mesopor. Mater.*, **295**, 109949 (2020).
170. M. D. McCluskey and S. J. Jokela, *J. Appl. Phys.*, **106**, 071101 (2009).
171. D. V. Brazhnyk, Y. P. Zaitsev, I. V. Bacherikova, V. A. Zazhigalov, J. Stoch and A. Kowal, *Appl. Catal. B: Environ.*, **70**, 557 (2007).
172. M. Seredych and T. J. Bandosz, *J. Phys. Chem. C*, **112**, 4704 (2008).
173. E.-K. Lee, K.-D. Jung, O.-S. Joo and Y.-G. Shul, *React. Kinet. Catal. Lett.*, **87**, 115 (2005).
174. N. Haimour, R. El-Bishtawi and A. Ail-Wahbi, *Desalination*, **181**, 145 (2005).
175. E. Laperdrix, G. Costent, O. Saur, J. C. Lavalley, C. Nédez, S. Sav-Poncet and J. Nougayrède, *J. Catal.*, **189**, 63 (2000).
176. X. Kan, X. Chen, W. Chen, J. Mi, J.-Y. Zhang, F. Liu, A. Zheng, K. Huang, L. Shen, C. Au and L. Jiang, *ACS Sustain. Chem. Eng.*, **7**, 7609 (2019).
177. Z. Yu, X. Wang, Y.-N. Hou, X. Pan, Z. Zhao and J. Qiu, *Carbon*, **117**, 376 (2017).
178. Y. Pan, M. Chen, M. Hu, M. Tian, Y. Zhang and D. Long, *Appl. Catal. B: Environ.*, **262**, 118266 (2020).
179. J.-D. Chai and M. Head-Gordon, *Phys. Chem. Chem. Phys.*, **10**, 6615 (2008).
180. F. Weigend and R. Ahlrichs, *Phys. Chem. Chem. Phys.*, **7**, 3297 (2005).
181. D. Long, Q. Chen, W. Qiao, L. Zhan, X. Liang and L. Ling, *Chem. Commun.*, **26**, 3898 (2009).
182. Q. Chen, J. Wang, X. Liu, X. Zhao, W. Qiao, D. Long and L. Ling, *Carbon*, **49**, 3773 (2011).
183. Q. Chen, Z. Wang, D. Long, X. Liu, L. Zhan, X. Liang, W. Qiao and L. Ling, *Ind. Eng. Chem. Res.*, **49**, 3152 (2010).
184. Z. Zhang, W. Jiang, D. Long, J. Wang, W. Qiao and L. Ling, *ACS Appl. Mater. Interfaces*, **9**, 2477 (2017).